

UK ammonia emissions estimated with satellite observations and GEOS-Chem

Eloise Ann Marais¹, Alok K Pandey², Martin Van Damme^{3,4}, Lieven Clarisse⁴, Pierre-Francois Coheur⁵, Mark W. Shephard⁶, Karen Cady-Pereira⁷, Tom Misselbrook⁸, Lei Zhu⁹, Gan Luo¹⁰, and Fangqun Yu¹¹

¹University College London

²University of Leicester

³Universite Libre de Bruxelles

⁴Universite libre de Bruxelles (ULB)

⁵Universite Libre de Bruxelles CP160/09

⁶Environment and Climate Change Canada

⁷Atmospheric and Environmental Research, Inc.

⁸Rothamsted Research Ltd

⁹School of Environmental Science and Engineering, Southern University of Science and Technology

¹⁰ASRC, SUNY-Albany

¹¹University at Albany

November 30, 2022

Abstract

Agricultural emissions of ammonia (NH₃) impact air quality, human health, and the vitality of aquatic and terrestrial ecosystems. In the UK, there are few direct policies regulating anthropogenic NH₃ emissions and development of sustainable mitigation measures necessitates reliable emissions estimates. Here we use observations of column densities of NH₃ from two space-based sensors (IASI and CrIS) with the GEOS-Chem model to derive top-down NH₃ emissions for the UK at fine spatial (~10 km) and time (monthly) scales. We focus on March-September when there is adequate spectral signal to reliably retrieve NH₃. We estimate total emissions of 272 Gg from IASI and 390 Gg from CrIS. Bottom-up emissions are 27% less than IASI and 49% less than CrIS. There are also differences in seasonality. Top-down and bottom-up emissions agree on a spring April peak due to fertilizer and manure application, but there is also a comparable summer July peak in the top-down emissions that is not in bottom-up inventories and appears to be associated with dairy cattle farming. We estimate relative errors in the top-down emissions of 11-36% for IASI and 9-27% for CrIS, dominated by column density retrieval errors. The bottom-up versus top-down emissions discrepancies estimated in this work impact model predictions of the environmental damage caused by NH₃ emissions and warrant further investigation.

UK ammonia emissions estimated with satellite observations and GEOS-Chem

Eloise A. Marais¹, Alok K. Pandey², Martin Van Damme³, Lieven Clarisse³, Pierre-François Coheur³, Mark W. Shephard⁴, Karen E. Cady-Pereira⁵, Tom Misselbrook⁶, Lei Zhu⁷, Gan Luo⁸, Fangqun Yu⁸

¹Department of Geography, University College London, London, UK.

²School of Physics and Astronomy, University of Leicester, Leicester, UK.

³Université libre de Bruxelles (ULB), Spectroscopy, Quantum Chemistry and Atmospheric Remote Sensing (SQUARES), Brussels, Belgium.

⁴Environment and Climate Change Canada, Toronto, Ontario, Canada.

⁵Atmospheric and Environmental Research (AER), Lexington, MA, USA.

⁶Department of Sustainable Agriculture Sciences, Rothamsted Research, Okehampton, UK.

⁷School of Environmental Science and Engineering, Southern University of Science and Technology, Shenzhen, China.

⁸Atmospheric Sciences Research Center, University at Albany, Albany, New York, USA.

Corresponding author: Eloise A. Marais (e.marais@ucl.ac.uk)

Key Points:

- Satellite observations of NH₃ from 2 sensors (IASI, CrIS) are used to estimate UK NH₃ emissions in Mar-Sep at fine scales (10 km, monthly)
- Satellite-derived NH₃ emissions total 272 Gg from IASI and 390 Gg from CrIS and exhibit a spring (April) and summer (July) peak
- Bottom-up inventories used for research and policy are 27-49% less than the satellite-derived estimates and miss the summer emissions peak

25 **Abstract**

26 Agricultural emissions of ammonia (NH_3) impact air quality, human health, and the vitality of
27 aquatic and terrestrial ecosystems. In the UK, there are few direct policies regulating
28 anthropogenic NH_3 emissions and development of sustainable mitigation measures necessitates
29 reliable emissions estimates. Here we use observations of column densities of NH_3 from two
30 space-based sensors (IASI and CrIS) with the GEOS-Chem model to derive top-down NH_3
31 emissions for the UK at fine spatial (~ 10 km) and time (monthly) scales. We focus on March-
32 September when there is adequate spectral signal to reliably retrieve NH_3 . We estimate total
33 emissions of 272 Gg from IASI and 390 Gg from CrIS. Bottom-up emissions are 27% less than
34 IASI and 49% less than CrIS. There are also differences in seasonality. Top-down and bottom-up
35 emissions agree on a spring April peak due to fertilizer and manure application, but there is also
36 a comparable summer July peak in the top-down emissions that is not in bottom-up inventories
37 and appears to be associated with dairy cattle farming. We estimate relative errors in the top-
38 down emissions of 11-36% for IASI and 9-27% for CrIS, dominated by column density retrieval
39 errors. The bottom-up versus top-down emissions discrepancies estimated in this work impact
40 model predictions of the environmental damage caused by NH_3 emissions and warrant further
41 investigation.

42 **Plain Language Summary**

43 Emissions of ammonia, mostly from agriculture, are often a dominant contributor to fine
44 particles in countries with well-established policies that have led to large reductions in other
45 precursors of such pollutants detrimental to our health. Here we use a model and observations of
46 ammonia from two space-based sensors to estimate emissions in the UK where there are no
47 direct policies regulating agricultural sources of ammonia. The satellite-derived emissions,
48 limited to March-September when conditions are ideal for viewing ammonia from space, total
49 272 kilotonnes from an instrument that passes overhead in the morning and 390 kilotonnes from
50 an instrument with a midday overpass. Though the emissions estimates differ for the two
51 instruments, both exhibit a spring (April) peak due to fertilizer and manure use and summer
52 (July) peak likely associated with dairy cattle farming. The summer peak is missing in bottom-up
53 emission inventories and total March-September emissions from these inventories are also 27-
54 49% less than those derived with satellites. Further research is needed to address these
55 discrepancies, as such inventories are widely used for developing policies and assessing
56 environmental damage caused by ammonia.

57 **1 Introduction**

58 Agricultural practices such as synthetic fertilizer and manure use and livestock farming
59 release large quantities of ammonia (NH_3) to the atmosphere. Once emitted, NH_3 partitions to
60 acidic aerosols to form ammonium that contributes to mass concentrations of fine particles
61 ($\text{PM}_{2.5}$) hazardous to health (Cohen et al., 2017; Dockery et al., 1993; Vohra et al., 2021a). NH_3
62 and ammonium also deposit to the Earth's surface and drastically alter the natural nitrogen
63 balance of terrestrial and aquatic ecosystems (Galloway, 1998; Johnson & Carpenter, 2010;
64 Vitousek et al., 1997).

65 In the UK, agriculture is the dominant ($>80\%$) source of NH_3 emissions (Ricardo, 2018a),
66 mostly from nitrogen fertilizer use, manure management, and farming of dairy and beef cattle
67 (DEFRA, 2019). Modelling studies suggest that the largest and most extensive decline in $\text{PM}_{2.5}$

68 in the UK would be achieved by targeting NH₃ sources (Vieno et al., 2016), but only large pig
69 and poultry farms are required to adopt best practices and technologies that reduce NH₃
70 emissions (DEFRA, 2019). There are additional policy options under consideration, such as
71 limiting the use of solid urea fertilizer, a large source of NH₃ in the UK (DEFRA, 2020a). As a
72 signatory of the United Nations Economic Commission for Europe (UNECE) Gothenburg
73 protocol, the UK is committed to an anthropogenic NH₃ emissions ceiling of 297 Gg, informed
74 by annual emissions estimates from the UK bottom-up National Atmospheric Emissions
75 Inventory (NAEI). The UK is also required as part of the protocol to reduce NH₃ emissions by
76 8% in 2020 and beyond relative to emissions in 2005 (UNECE, 2019). The estimated decline in
77 NH₃ emissions from 1980 to 2017 is 0.2% a⁻¹ due to a steep decline in vehicular emissions of
78 NH₃ in 1998-2007 and a recent increase in agricultural emissions since 2013 (Ricardo, 2020).
79 Any future policies targeting NH₃ emissions would also need to consider increases in emissions
80 as the atmosphere warms (Sutton et al., 2013).

81 Estimates of the contribution of NH₃ emissions to PM_{2.5} and mobilization of nitrogen in
82 aquatic and terrestrial ecosystems, assessment of attainment of UNECE emissions ceilings and
83 trends, and decisions on effective mitigation measures demand accurate estimates of NH₃
84 emissions. The NAEI of annual total and mapped UK NH₃ emissions is published each year.
85 These are at high spatial resolution (1 km) and incorporate detailed information about the
86 farming activities that contribute to NH₃ emissions. The ability to validate the inventory is
87 challenging, as there are no long-term measurements of NH₃ fluxes. There is a network of very
88 reliable measurements of rural 24-hour mean surface concentrations of NH₃ that cover the full
89 latitudinal extent of the UK from Cornwall in the south to Shetland in the north (Tang et al.,
90 2018), but there are large monitoring gaps in-between. Satellite observations of NH₃ retrieved
91 from infrared spectral measurements offer complete coverage of the UK and routine daily
92 measurements in the absence of clouds and under good retrieval conditions. Satellites observe
93 NH₃ molecules throughout the atmospheric column, but the majority are within the planetary
94 boundary layer and most of the variability in the column is typically due to NH₃ at or near the
95 surface (Clarisse et al., 2010; Nowak et al., 2010; Schiferl et al., 2016; Vohra et al., 2021b).

96 Retrieval of NH₃ from space-based instruments was first described by Beer et al. (2008)
97 for the Tropospheric Emission Spectrometer (TES) instrument. Satellite NH₃ retrieval products
98 have since undergone substantial retrieval development (Clarisse et al., 2009; Shephard et al.,
99 2011; 2020; Shephard & Cady-Pereira, 2015; Van Damme et al., 2014b; 2017; 2021; Whitburn
100 et al., 2016a), intercomparisons (Dammers et al., 2019), and validation against ground-based
101 observations of total atmospheric column densities and surface concentrations of NH₃ (Dammers
102 et al., 2016; 2017; Van Damme et al., 2015a; Vohra et al., 2021b). These products have also seen
103 extensive use in characterizing NH₃ emissions. This includes detecting global and regional NH₃
104 emission hotspots (Cady-Pereira et al., 2017; Clarisse et al., 2019; Dammers et al., 2019;
105 Shephard et al., 2020; Van Damme et al., 2018), constraining NH₃ emissions from biomass
106 burning (Adams et al., 2019; Whitburn et al., 2016b), evaluating regional emission inventories
107 (Chen et al., 2021; Fortems-Cheiney et al., 2020), identifying underestimated or missing NH₃
108 sources in widely used global and regional emission inventories and models (Heald et al., 2012;
109 Hickman et al., 2018; Van Damme et al., 2014a), and determining long-term local and regional
110 trends and variability in NH₃ (Hickman et al., 2020; Van Damme et al., 2015b; 2021; Vohra et
111 al., 2021b; Wichink Kruit et al., 2017).

112 Here we use satellite observations of NH₃ and the GEOS-Chem chemical transport model
113 (CTM) to derive top-down NH₃ emissions for the UK and evaluate the bottom-up NAEI
114 emissions inventory and current understanding of seasonality in emissions. This includes the use
115 of surface observations from the UK monitoring network to evaluate GEOS-Chem and
116 corroborate findings from the satellite observations.

117 **2 Space-based observations of column densities of NH₃**

118 Satellite observations of NH₃ retrieved in the infrared portion of the light spectrum rely
119 on the spectral signal that depends on the atmospheric state, such as abundance and vertical
120 distribution of NH₃ and thermal contrast between the surface of the Earth and the overlying
121 atmosphere (Clarisse et al., 2010; Shephard et al., 2011). Two prominent products are available
122 from contemporary space-based instruments that pass overhead in the morning (the Infrared
123 Atmospheric Sounding Interferometer or IASI) and midday (the Cross-track Infrared Sounder or
124 CrIS). These products use distinct retrieval approaches for us to assess the constraints these
125 provide on NH₃ emissions in the UK.

126 **2.1 Infrared Atmospheric Sounding Interferometer NH₃**

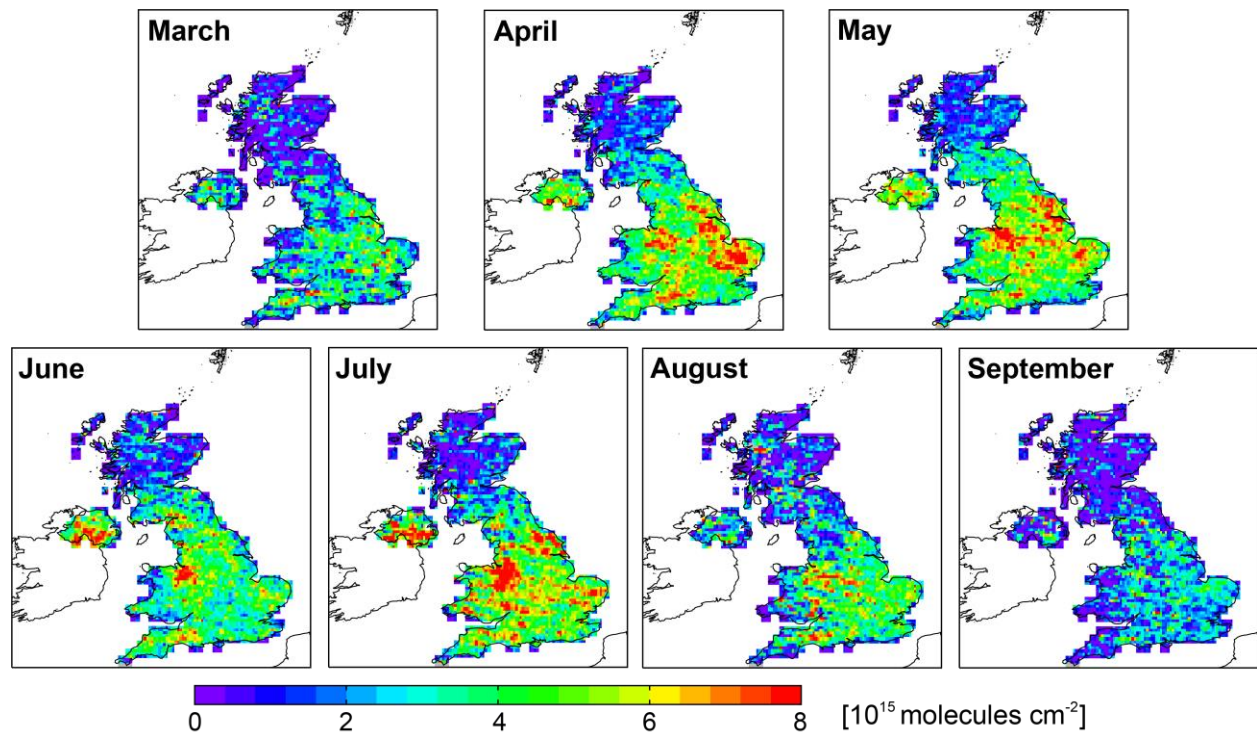
127 The IASI instrument onboard the Metop-A satellite was launched into low-Earth polar
128 sun synchronous orbit in October 2006. The instrument has two overpass times in the morning
129 (09h30 local solar time or LST) and at night (21h30 LST), providing global coverage twice a
130 day. The elliptical IASI pixels range in ground pixel resolution from 12 km × 12 km at nadir
131 (directly below the instrument) to about 20 km × 39 km at the edges of the 2200-km-wide swath
132 (Clarisse et al., 2011). The data product we use is the Level 2 cloud-free reanalysis product of
133 total column NH₃ (version 3R-ERA5) (Van Damme et al., 2021). The retrieval uses machine
134 learning, specifically a neural network trained relationship between column NH₃ and a so-called
135 hyperspectral range index or HRI, where the HRI is a measure of the relative enhancement in the
136 spectral signature due to NH₃ (Van Damme et al., 2014b; 2017; Whitburn et al., 2016a). The data
137 product includes reported retrieval errors estimated by perturbing individual input parameters in
138 the neural network framework (Whitburn et al., 2016a). The neural network retrieved product
139 has been validated against global and regional networks of ground-based NH₃ observations of
140 surface concentrations and column densities (Dammers et al., 2016; Guo et al., 2021; Vohra et
141 al., 2021b; Whitburn et al., 2016a). In general, IASI NH₃ reproduces the temporal variability in
142 surface concentrations of NH₃, but exhibits a low bias of 25-50% (Dammers et al., 2017;
143 Whitburn et al., 2016a).

144 We use daytime (09h30 LST) IASI NH₃ for 2008-2018 to obtain multiyear monthly
145 means. This dampens influence of interannual variability and ensures consistency with NAEI
146 NH₃ emissions that are estimated with 30-year mean meteorology (Ricardo, 2019b). We grid the
147 data to finer spatial resolution (0.1° × 0.1°) than the native resolution of the instrument using the
148 tessellation oversampling technique described in Zhu et al. (2017) and Sun et al. (2018). This
149 takes advantage of the spatial variability in coverage of individual orbits and the long data record
150 from IASI to reduce noise and smooth out spatial gradients in the gridded product (Sun et al.,
151 2018). Briefly, tessellation involves weighting individual IASI pixels by the area of overlap with
152 the target grid and also includes error-weighting using the reported retrieval error. In our
153 application of the tessellation gridding technique, we approximate the area of IASI pixels as a

154 quadrilateral polygon, where the corners of each polygon are estimated as the distance midway
 155 between the centres of neighbouring IASI pixels.

156 Retrieval of NH_3 over the UK is challenging, due to persistent clouds and relatively cool
 157 conditions. Extreme retrievals, identified as absolute columns $> 5 \times 10^{17}$ molecules cm^{-2} , are
 158 removed. We also exclude IASI NH_3 columns retrieved on 26-27 July 2018, coincident with the
 159 summer 2018 heat wave (McCarthy et al., 2019). Record high temperatures ($> 30^\circ\text{C}$) lead to UK
 160 IASI NH_3 column densities 4-times greater ($\sim 4 \times 10^{16}$ molecules cm^{-2}) than the UK July
 161 multiyear mean ($\sim 1 \times 10^{16}$ molecules cm^{-2}) and cause an 11% positive bias in the July multiyear
 162 mean. A similarly large influence of heat waves on IASI NH_3 columns resulted from the summer
 163 2010 heat wave over mainland Europe (Van Damme et al., 2014a). Following oversampling, the
 164 gridded multiyear means with large relative error ($> 50\%$) are removed. This leads to loss of the
 165 majority of IASI NH_3 columns in October-February, so only March-September multiyear means
 166 are considered. According to the monthly NH_3 emissions estimated by Hellsten et al. (2007),
 167 March-September accounts for $\sim 60\%$ of the annual total. Additional outlier filtering is applied to
 168 the gridded multiyear monthly means to remove columns $< -1 \times 10^{16}$ molecules cm^{-2} and $> 1 \times$
 169 10^{17} molecules cm^{-2} . These account for $< 0.1\%$ of the March-September data.

170



171

172 **Figure 1.** Monthly multiyear (2008-2018) mean IASI NH_3 . Data are gridded to $0.1^\circ \times 0.1^\circ$ using
 173 oversampling (see text for details). Grey grids have < 10 observations.

174 Figure 1 shows the gridded March-September multiyear monthly mean IASI NH_3
 175 columns. The number of observations in each grid ranges from 11 to 128. Values over Scotland
 176 are very low (typically $< 2 \times 10^{15}$ molecules cm^{-2}) due to weak signal and lower agricultural

177 activity than the rest of the UK. The range in IASI NH_3 over the rest of the country of $4\text{--}8 \times 10^{15}$
178 molecules cm^{-2} is much less than the NH_3 hotspots in other parts of the world. Columns over
179 global hotspots such as North China, West Africa, the Po Valley (Italy), and the Indo-Gangetic
180 Plain (India) exceed 2×10^{16} molecules cm^{-2} (Cady-Pereira et al., 2017; Dammers et al., 2019;
181 Van Damme et al., 2014a; 2018). These are associated with industrial and agricultural activity in
182 India and China and intense seasonal open burning of biomass in West Africa and northern India,
183 aided by warm temperatures increasing NH_3 emissions and enhancing the spectral signal.

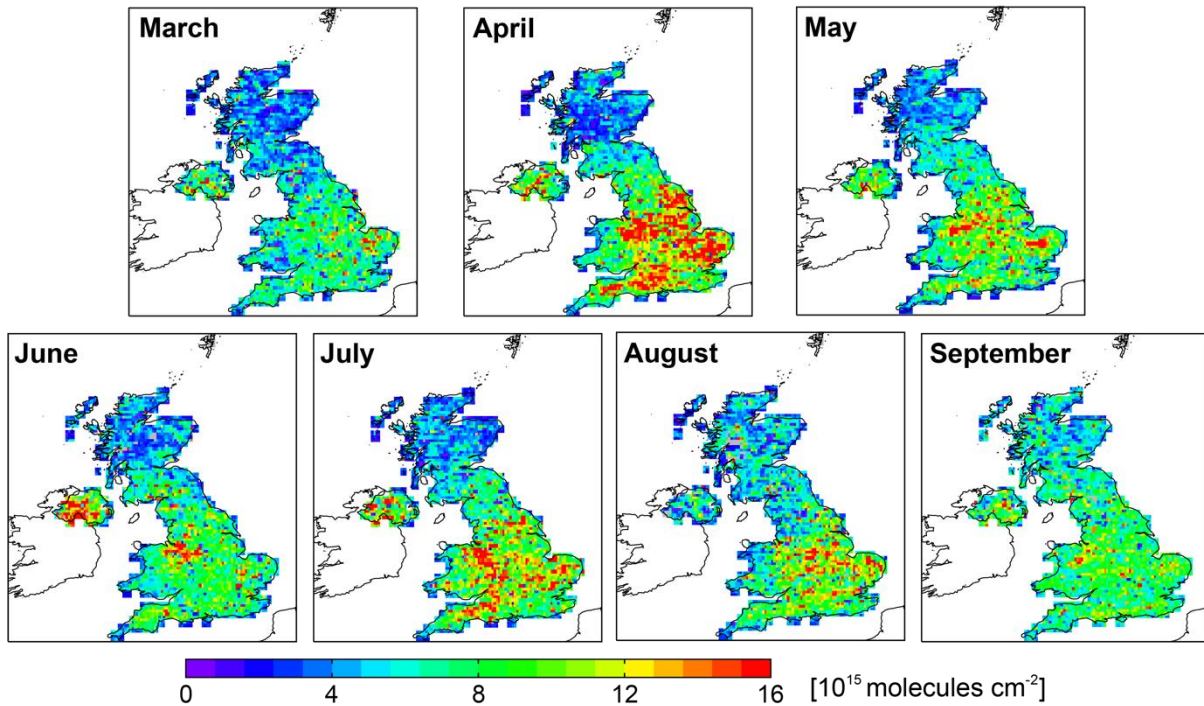
184 **2.2 Cross-track Infrared Sounder NH_3**

185 The first CrIS sensor launched into low-Earth polar sun synchronous orbit in October
186 2011 is onboard the NOAA Suomi-NPP satellite. Like IASI, CrIS observes the Earth twice daily,
187 though in the early afternoon (13h30 LST) and after midnight (01h30 LST) (Goldberg et al.,
188 2013). It has the same swath width as IASI and similar ground pixel resolution (14 km circular
189 pixels at nadir). The fast physical retrieval (CFPR) approach used to retrieve NH_3 columns is
190 described in detail in Shephard & Cady-Pereira (2015) and Shephard et al. (2020). Briefly, it is
191 based on conventional optimal estimation that involves minimizing the difference between
192 observed and calculated outgoing spectral radiances with a priori vertical profiles of NH_3
193 (Rodgers, 2000). CFPR uses three prior NH_3 profiles representing polluted, moderately polluted,
194 and remote conditions (Shephard et al., 2020) that are selected based on the ammonia spectral
195 signal. This is different to standard optimal estimation that uses prior information that is
196 independent of the observations and imposes spatial and temporal information. The CFPR
197 retrieval generates averaging kernels that quantify the vertical sensitivity of the retrieval. These
198 typically peak between 900 and 750 hPa ($\sim 1\text{--}2.5$ km altitude) (Dammers et al., 2017; Shephard &
199 Cady-Pereira, 2015).

200 We use the Level 2 CrIS NH_3 CFPR version 1.6 product for 2013-2018. The predecessor
201 product (version 1.5) exhibited a positive bias for $\text{NH}_3 < 1 \times 10^{16}$ molecules cm^{-2} , as values were
202 only retrieved over scenes exceeding the instrument detection limit of $\sim 2 \times 10^{15}$ molecules cm^{-2}
203 (Dammers et al., 2017; Shephard & Cady-Pereira, 2015). This approach filtered out cloud-free
204 scenes below the instrument detection limit and indirectly removed cloudy scenes when the NH_3
205 signal below clouds could not be detected. In version 1.6 clouds are explicitly identified with
206 information from the space-based Visible Infrared Imaging Radiometer Suite (VIIRS) (White et
207 al., 2021). We use daytime cloud-free CrIS observations with quality flag ≥ 4 (Shephard et al.,
208 2020) and thermal contrast > 0 K, where thermal contrast is the difference between the reported
209 temperatures at the surface and the lowest atmospheric layer. We identify and correct for a
210 positive trend in the CrIS baseline that appears to be erroneous, as it is not apparent in the IASI
211 data. We do this by estimating a statistically significant (p-value = 0.02) increase in monthly
212 mean background NH_3 columns over Scotland (Figure S1) of 2.33×10^{13} molecules cm^{-2} per
213 month (amounting to 1.7×10^{15} molecules cm^{-2} over the whole record) and subtract this from
214 individual CrIS NH_3 column retrievals. We grid the corrected data to $0.1^\circ \times 0.1^\circ$ using the same
215 tessellation code used for IASI, but without error weighting. The individual total column errors
216 include measurement and representative errors and cover a much narrower range (5-55%
217 (Shephard et al., 2020)) than those for IASI (5% to $>100\%$). As a result, higher relative
218 weighting would be applied to low column densities, leading to anomalously low gridded values
219 in the CrIS multiyear means. For consistency with IASI, we only consider March to September.

220 Figure 2 shows the gridded March-September CrIS NH₃ multiyear monthly mean
 221 columns. As with IASI, we filter for outliers in the multiyear means (column densities $< -1 \times$
 222 10^{16} molecules cm⁻² and $> 1 \times 10^{17}$ molecules cm⁻²), removing $< 0.1\%$ of the gridded data. Unlike
 223 IASI, the observations during the July 2018 heatwave only increase the July multiyear mean by
 224 1.6%, so these days are retained. The number of CrIS retrievals in each grid ranges from 11 to
 225 96. The CrIS multiyear means are roughly double those for IASI (Figure 1), in part because CrIS
 226 passes overhead at midday when higher ambient temperatures lead to greater volatilization of
 227 NH₃. Differences in vertical sensitivity and distinct retrieval approaches likely also contribute.
 228 This difference is particularly large in September when background NH₃ is 5.3×10^{15} molecules
 229 cm⁻² more in CrIS than IASI, obtained as the intercept from regressing CrIS against IASI. The
 230 spatial correlation between CrIS and IASI multiyear means is $R < 0.5$ in most months (March,
 231 June-September), $R = 0.53$ in May, and $R = 0.55$ in April.

232



233

234

235 **Figure 2.** Monthly multiyear (2013-2018) mean CrIS NH₃. Data are gridded to $0.1^\circ \times 0.1^\circ$ with
 236 oversampling (see text for details). Grey grids have < 10 observations.

237 3 The GEOS-Chem chemical transport model

238 We use the GEOS-Chem CTM version 12.1.0 (<https://doi.org/10.5281/zenodo.1553349>)
239 to interpret constraints on UK NH₃ emissions from IASI and CrIS. The model is driven with
240 NASA GEOS-FP assimilated meteorology from the Global Modeling and Assimilation Office
241 (GMAO). Model simulations are conducted on a horizontal grid at 0.25° × 0.3125° (latitude ×
242 longitude) nested over western Europe (32.75-61.25°N, 15°W-40°E). The model extends over 47
243 vertical layers from the Earth's surface to 0.01 hPa. Dynamic (3-hourly) boundary conditions are
244 from a global GEOS-Chem simulation at 4° × 5°.

245 Anthropogenic emissions over the UK, including from agriculture, are updated in GEOS-
246 Chem to include gridded emissions from the NAEI for 2016 (Ricardo, 2018b). These are annual
247 totals on a 1 km × 1 km grid available at <https://naei.beis.gov.uk/data/map-uk-das> (last accessed
248 August 2019). The agricultural NH₃ emissions incorporated in the NAEI are calculated at coarser
249 resolution (5 km) than the NAEI with the nitrogen balance models of Webb & Misselbrook
250 (2004) for livestock sources and Misselbrook et al. (2006) for fertilizer sources. These models
251 are driven with 30-year mean meteorology for 1981-2010, so the NH₃ emissions represent a
252 climatological mean (Ricardo, 2019b). Other anthropogenic NH₃ emissions are typically
253 calculated as the product of emission and activity factors representative of the year of interest
254 and mapped to the 1 km NAEI emissions grid (Ricardo, 2018a). Temporal variability of annual
255 NAEI NH₃ emissions is represented in GEOS-Chem with gridded monthly scaling factors
256 already included in the model and spatially uniform diurnal scaling factors calculated by Zhu et
257 al. (2015) using information about the dependence of NH₃ on aerodynamic resistance, surface
258 temperature and Henry's law. As a result of these, 30% of NH₃ is emitted at midday (noon-2pm
259 LST) coincident with the CrIS overpass and 20% in the morning (9am-noon LST) coincident
260 with the IASI overpass. Monthly scaling factors are from gridded data derived by Friedrich
261 (2000) and lead to peak NH₃ emissions in April. Natural NH₃ sources are from inventories
262 already in GEOS-Chem. These include natural emissions from soils and the ocean from the
263 Global Emissions Initiative (GEIA) inventory (Bouwman et al., 1997) and inland and coastal
264 seabird emissions from the Riddick et al. (2012) inventory. We halve the GEIA inventory
265 emissions, as in Paulot et al. (2014), informed by a 50% overestimate identified by Simpson et
266 al. (1999).

267 NH₃ is a semi-volatile acid buffer that neutralizes acidic sulfate and nitrate aerosols, so
268 its abundance depends on the abundance of these acidic aerosols. Sulfate forms from oxidation
269 of SO₂ and nitrates from aerosol uptake of nitric acid formed from oxidation of NO_x. The version
270 of the NAEI we use includes outdated mapping of the location of ships and no vertical or
271 temporal information for aircraft emissions. To address these issues, we separate ship and
272 aircraft emissions from other sources in the lumped "Other Transport and Mobile Machinery"
273 category of the NAEI emissions inventory and replace ship emissions with updated estimates
274 that use geospatial information from the automatic identification system (Ricardo, 2017). We
275 convert the NAEI aircraft emissions to monthly estimates and distribute these vertically up to 1
276 km (the altitude limit of the NAEI emissions) by deriving vertical and temporal scaling factors
277 from the global Aviation Emissions Inventory version 2.0 (AEIv2) used in GEOS-Chem (Stettler
278 et al., 2011). Above 1 km, the AEIv2 emissions are used. The existing temporal scaling factors in
279 GEOS-Chem that are applied to NAEI SO₂ and NO_x emissions lead to peak emissions in winter,
280 due to an increase in energy demand. SO₂ is emitted in the model as 95% SO₂ and 5% sulfate,

281 using sulfate-to-SO₂ emission ratios for Europe reported by Chin et al. (2000). NAEI emissions
282 are gridded to a uniform 0.1° × 0.1° grid for input to the Harmonized Emissions Component
283 (HEMCO) processing package version 2.1.010 (Keller et al., 2014) that maps all emissions to the
284 model grid and applies relevant scaling factors.

285 The model includes detailed coupled gas- and aerosol-phase chemistry. Sulfate aerosols
286 are formed in the model from oxidation of SO₂ in the gas phase by OH and in the aqueous phase
287 in clouds by ozone and hydrogen peroxide (Park et al., 2004). Partitioning of NH₃ between the
288 gas and acidic aerosol phase is determined dynamically with the thermodynamic equilibrium
289 model ISORROPIA-II (Fountoukis & Nenes, 2007). Wet and dry deposition, terminal sinks of
290 NH₃, are represented with a standard resistances-in-series scheme for dry deposition (Wesley et
291 al., 1998) and, for wet deposition, includes scavenging in and below clouds (Amos et al., 2012).

292 We use network site measurements of trace gases and aerosols to evaluate model
293 accuracy at reproducing surface concentrations of NH₃, SO₂, and sulfate. These include 2 rural
294 sites (Auchencorth Moss in Scotland, Chilbolton Observatory in southern England) that form
295 part of the European Monitoring and Evaluation Programme (EMEP) network and the mostly
296 rural UK Eutrophying and Acidifying Atmospheric Pollutants (UKEAP) network. The 2 EMEP
297 sites include hourly measurements from Monitor for AeRosols and Gases in Air (MARGA)
298 instruments (Stieger et al., 2017; ten Brink et al., 2007; Twigg et al., 2015; Walker et al., 2019).
299 The UKEAP network sites include monthly measurements from low-cost denuder filter sampling
300 packs (Tang et al., 2018). The MARGA data are from the EMEP Chemical Coordinating Centre
301 EBAS database (<http://ebas.nilu.no/>; last accessed February 2020) (Tørseth et al., 2012) and the
302 UKEAP data are from the UK-AIR data archive (<https://uk-air.defra.gov.uk/data/data-availability>;
303 last accessed November 2020).

304 To ensure consistency between the model and observations, the model is sampled from
305 the lowest to the top model layer during satellite overpasses for comparison to IASI (08-11 LST)
306 and CrIS (12-15 LST), and as monthly 24-hour means in the lowest model layer for comparison
307 to the surface observations. The model is sampled in March-September 2016 following a 2-
308 month spin-up for chemical initialization.

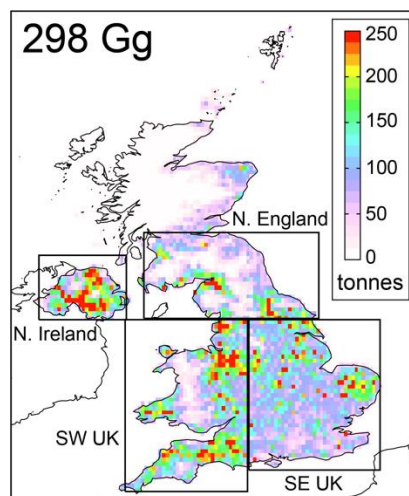
309 **4 UK bottom-up emissions of NH₃**

310 Figure 3 shows the spatial distribution of annual UK NH₃ emissions for 2016 from the
311 NAEI. Table 1 gives the breakdown by sector. Annual emissions for 2016 total 298 Gg, mostly
312 (84%) from agriculture. Natural emissions of 21.6 Gg (7% of the total) are consistent with
313 annual total natural emissions in GEOS-Chem of 21.8 Gg. According to GEOS-Chem, these
314 include soils, vegetation and the ocean (together 18.7 Gg) and seabirds (3.10 Gg). NAEI
315 anthropogenic NH₃ emissions total 276 Gg, 21 Gg less than the UNECE Gothenburg protocol
316 emissions ceiling of 297 Gg (UNECE, 2019). The NAEI version we implement in GEOS-Chem
317 and evaluate against top-down estimates was released in 2018. Two NAEI versions have been
318 released since. Reported differences in NH₃ emissions across these versions for consistent years
319 is minor, just 1-3% (Ricardo, 2019a; 2020).

320 The spatial patterns in Figure 3 coincide with farming activities that dominate NH₃
321 emissions according to the modelling study by Hellsten et al. (2008) that uses the same Webb &

322 Misselbrook (2004) nitrogen balance model as the NAEI. Dominant agricultural sources include
 323 sheep farming along the Welsh border where emissions are low, and large sources like pig and
 324 poultry farming and fertilizer use in east England and dairy and beef cattle farming in west
 325 England and Northern Ireland. Hellsten et al. (2008) used agricultural activity data for 2000.
 326 Detailed geospatial farming activity data is proprietary and publicly available data are limited to
 327 decadal maps of farming activities in England for 2000 and 2010 and annual regional and
 328 national statistics. The decadal maps suggest that locations of intensive crop and livestock
 329 farming in England are relatively unchanged (DEFRA, 2016b; a). The regional statistics
 330 document large changes in the number of livestock and the amount of nitrogen fertilizer used
 331 from 2000 to 2016 that would affect trends in emissions. In general, livestock numbers in the UK
 332 have declined by 20% for sheep, 11% for dairy and beef cattle, and 25% for pigs (DEFRA,
 333 2020b). Poultry, specifically table chickens, have increased by 10% in the UK, with the largest
 334 increase of 42% in Northern Ireland (DEFRA, 2020b). Nitrogen-based fertilizer usage, a
 335 dominant NH_3 source in east England (Hellsten et al., 2008), declined by 19% in the UK, ranging
 336 from a 3% increase in Scotland to a 37% decrease in Northern Ireland (AIC, 2020).

337



338

339

340 **Figure 3.** Annual UK NH_3 emissions for 2016. Data are in tonnes per year from the NAEI
 341 gridded to $0.1^\circ \times 0.1^\circ$. Inset value is the UK annual total. Boxes demarcate regions with broadly
 342 similar NH_3 sources: Northern Ireland (N. Ireland), Northern England and a portion of southern
 343 Scotland (N. England), southwest UK (SW UK), and southeast UK (SE UK).

344

345 **Table 1.** UK sector emissions of NH_3 according to the NAEI ^a

Sources	NH_3 [Gg a^{-1}]
Agriculture	248.9
Natural ^b	21.6
Waste	14.2
Point sources	4.4
Road transport	4.4

Other ^c	4.2
Total	297.7

346 ^a Spatial distribution of UK NAEI NH₃ emissions are in Figure 3. ^b Contributors to natural emissions,
 347 according to GEOS-Chem, are soils, vegetation and the ocean (together 18.7 Gg) and seabirds (3.1 Gg). ^c Other
 348 is industrial and domestic combustion (2.9 Gg) and solvent use (1.3 Gg).

349 Inversion of column densities of NH₃ to estimate top-down surface emissions can be
 350 complicated by dependence of NH₃ abundance on acidic sulfate aerosols formed from oxidation
 351 of SO₂. UK SO₂ emissions are dominated by large industrial and energy sector point sources,
 352 ships, domestic and industrial combustion, and traffic (Ricardo, 2018a). We find that monthly
 353 mean March-September 2016 GEOS-Chem SO₂ concentrations driven with the NAEI are much
 354 greater than those measured at EMEP and UKEAP network sites (Figure S2). The model
 355 normalized median bias is >500% for modelled SO₂ > 2 μg m⁻³ at sites influenced by point
 356 sources in Yorkshire and ~280% for modelled SO₂ < 2 μg m⁻³. Modelled sulfate is also greater
 357 than the observations (normalized mean bias or NMB of 17%) (Figure S2). This would enhance
 358 partitioning of NH₃ to acidic aerosols to form ammonium, leading to a positive bias in the
 359 relative amount of NH_x (NH₃ + ammonium) present as ammonium.

360 Positive model biases in both SO₂ and sulfate (Figure S2) suggest an overestimate in
 361 NAEI SO₂ emissions, though other factors may contribute. These include, but are not limited to,
 362 misrepresentation of the height at which SO₂ is emitted from tall stacks, a reported positive bias
 363 in mainland Europe SO₂ emissions (Luo et al., 2020), and uncertainties in wet deposition (Luo et
 364 al., 2019). We conducted sensitivity simulations to assess the contribution of these uncertainties
 365 to modelled SO₂ and sulfate. Details of these simulations and the effect on SO₂ and sulfate
 366 concentrations are in the accompanying Supplementary. The factor we find to have the largest
 367 influence relative to the model bias is wet deposition. The more efficient wet deposition scheme
 368 of Luo et al. (2019) leads to an 11% decrease in sulfate concentrations.

369 Errors in NAEI SO₂ emissions could be due to uncertainties in emissions from domestic
 370 and industrial biomass combustion. The third of six generating units at the 3.9 GW generating
 371 capacity Drax power station in Yorkshire transitioned from burning coal to biomass in 2016
 372 (Simet, 2017). SO₂ emissions from biomass combustion depend on fuel sulfur content and
 373 combustion efficiency. Reported emission factors range widely from 1 to 110 mg SO₂ MJ⁻¹
 374 (Boersma et al., 2008; Paulrud et al., 2006) and so offer limited constraints. To reduce the
 375 influence of a possible bias in SO₂ emissions on GEOS-Chem simulation of abundance of sulfate
 376 and NH₃, we decrease land-based gridded (0.1° × 0.1°) NAEI SO₂ emissions by a factor of 3 for
 377 grids dominated by point sources (identified as grids with SO₂ emissions > 10 g m⁻² a⁻¹) and by a
 378 factor of 1.3 for all other land-based grids. This reduces the original NAEI SO₂ emissions over
 379 land by 49% from 164 Gg to 84.1 Gg. With shipping, the updated annual NAEI SO₂ emissions
 380 for the domain shown in Figure 3 total 94.5 Gg. The March-September modelled sulfate NMB
 381 changes from +17% (Figure S2) to -8.8%. We use the scaled SO₂ emissions in all subsequent
 382 simulations.

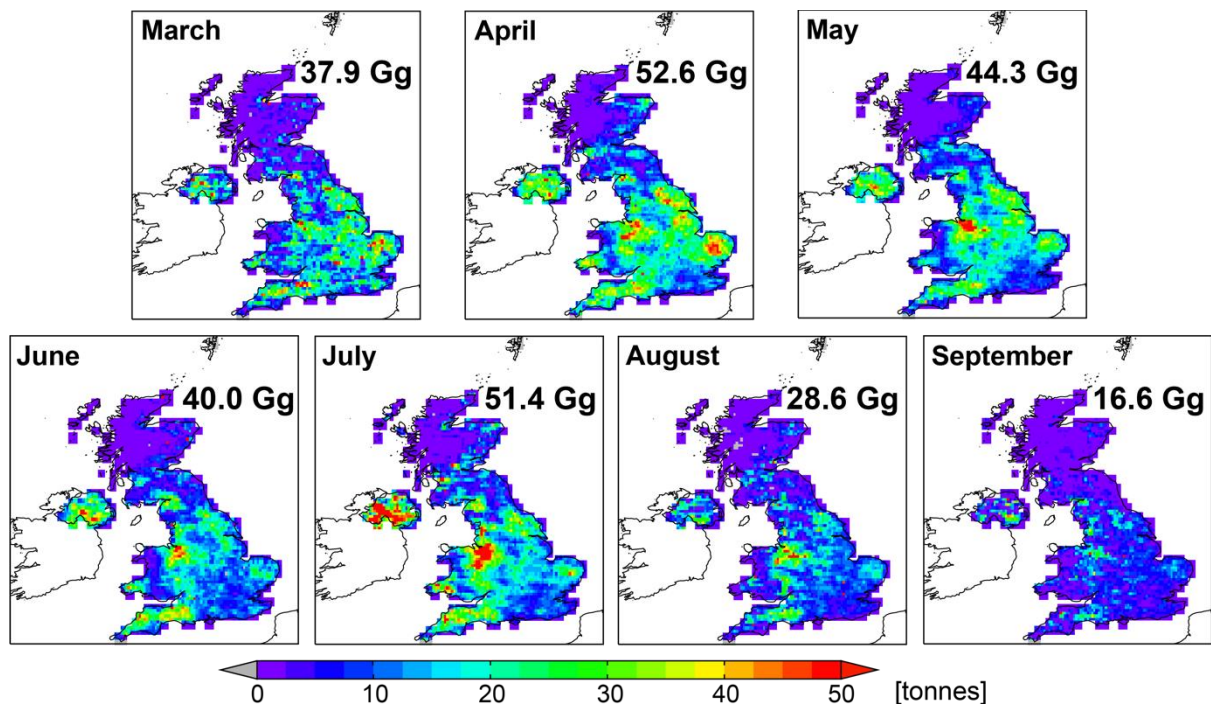
383 **5 Top-down NH₃ emissions and comparison to bottom-up estimates**

384 We calculate top-down NH₃ emissions by multiplying the satellite NH₃ multiyear
 385 monthly mean columns (Figure 1 for IASI, Figure 2 for CrIS) by GEOS-Chem ratios of 24-hour

386 mean NH_3 emissions to 3-hour mean columns (08-11 LST for IASI, 12-15 LST for CrIS) after
 387 interpolating the model fields to $0.1^\circ \times 0.1^\circ$. The mass-balance approach that we use to infer
 388 emissions can be susceptible to spatial misattribution of emissions due to displacement of NH_3
 389 from the source. The global mean lifetime of NH_3 is ~ 15 h (Hauglustaine et al., 2014), ranging
 390 from ~ 2 h near large sources (Dammers et al., 2019) to ~ 36 h far from emission sources (Van
 391 Damme et al., 2018). The displacement length, the distance for NH_3 to decay to $\sim 63\%$ of the
 392 original concentration of the emission source (Marais et al., 2012; Palmer et al., 2003), is similar
 393 to the resolution of the satellite-derived emissions (10-12 km) for calm conditions (wind speeds
 394 of $5\text{-}6 \text{ km h}^{-1}$) and short NH_3 lifetimes (2 h). Conditions are relatively stable in the UK in
 395 summer (Figure A1f.3 of BEIS (2016)), so meteorological mean wind speeds typically reach ~ 7
 396 km h^{-1} . At these slightly windier conditions and for a longer NH_3 lifetime of 15 h, the
 397 displacement length increases to 105 km.

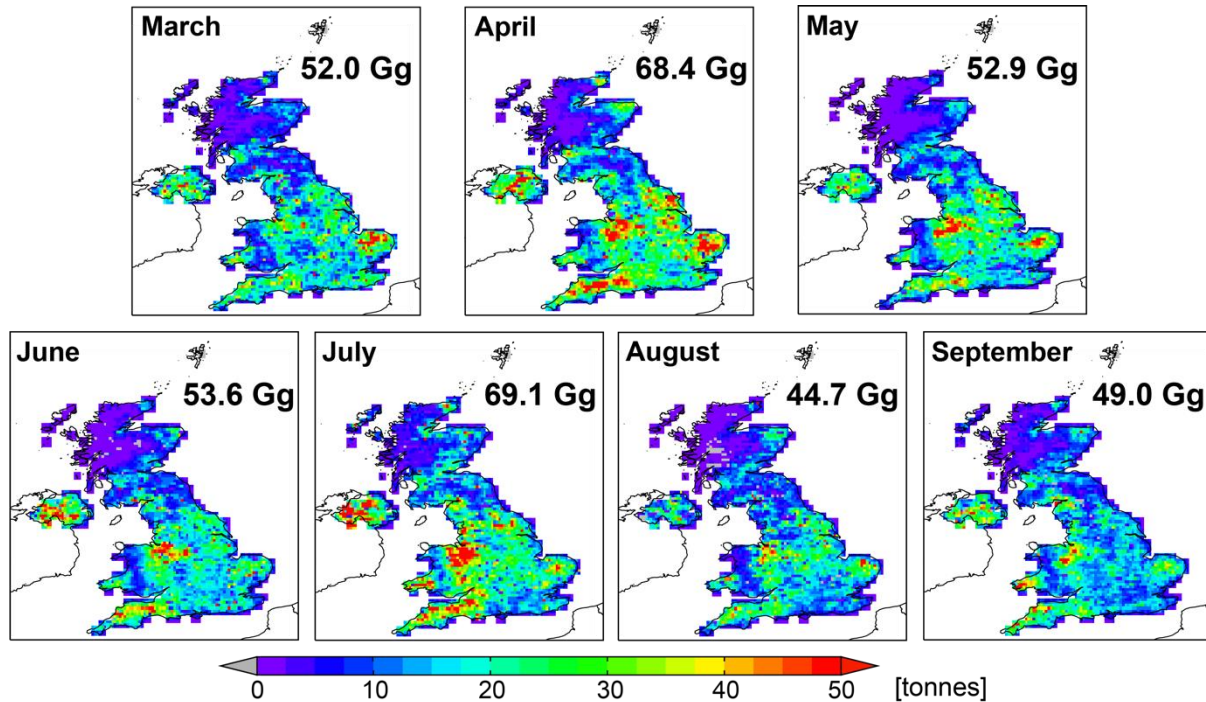
398 Maps of the resultant top-down monthly NH_3 emissions are shown in Figure 4 for IASI
 399 and Figure 5 for CrIS. Emissions for retained grid squares total 271.5 Gg for IASI, whereas these
 400 are 44% more from CrIS (389.6 Gg). CrIS monthly emissions are 19-37% more than IASI for
 401 March-July, similar in magnitude to the reported 25-50% low bias in IASI columns (Dammers et
 402 al., 2017; Whitburn et al., 2016a). The percentage difference increases to 56% for August and
 403 $>100\%$ for September. The large difference in September is due to 5.3×10^{15} molecules cm^{-2}
 404 greater background NH_3 in CrIS, even after correcting for the baseline trend (Section 2.2, Figure
 405 S1). CrIS emissions excluding September are 34% more than IASI. Qualitatively, both estimates
 406 exhibit similar spatial patterns to the NAEI (Figure 3). This includes relatively low emissions
 407 along the Welsh border, and peak emissions in Northern Ireland, the northern portion of the
 408 English side of the Welsh border, and in Norfolk in the east.

409



410

411 **Figure 4.** IASI-derived NH_3 emissions for March-September. Maps are at $0.1^\circ \times 0.1^\circ$. Inset
 412 values are monthly emissions that sum to 271.5 Gg.
 413



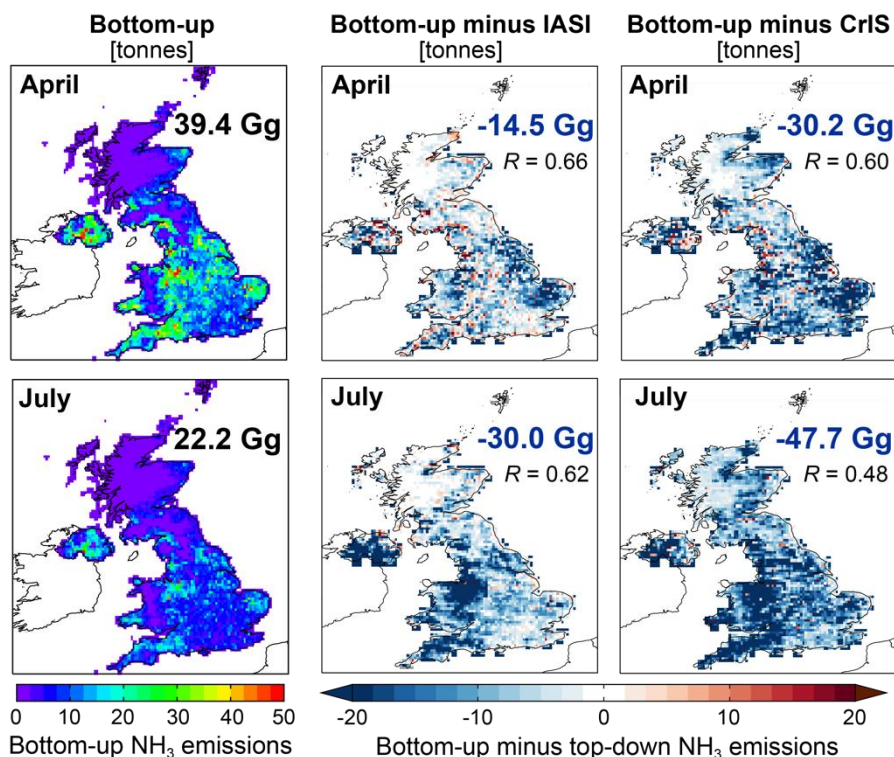
414
 415
 416 **Figure 5.** CrIS-derived NH_3 emissions for March-September. Maps are at $0.1^\circ \times 0.1^\circ$. Inset
 417 values are monthly emissions that sum to 389.6 Gg.

418 For comparison of monthly top-down and bottom-up emissions, we estimate bottom-up
 419 emissions as the product of the annual NAEI emissions in Figure 3 and ratios of GEOS-Chem
 420 monthly to annual NH_3 emissions interpolated onto the $0.1^\circ \times 0.1^\circ$ grid. Figure 6 shows the
 421 resultant monthly bottom-up NH_3 emissions for April and July. The other months are in the
 422 supplementary (Figure S3). The bottom-up emissions peak in April (~14% of the annual total)
 423 coincident with fertilizer application (Hellsten et al., 2007; Paulot et al., 2014). The gridded
 424 difference between top-down and bottom-up emissions are also shown in Figure 6 for April and
 425 July and Figure S3 for the other months. Locations where bottom-up emissions exceed those
 426 from the top-down approach (red grids) mostly occur where emissions are low. The largest
 427 difference is in July when top-down emissions are 30 Gg more (IASI) and 48 Gg more (CrIS)
 428 than the bottom-up inventory. Pronounced regional differences include lower bottom-up values
 429 in eastern England, particularly in April, where fertilizer use and pigs and poultry farming are
 430 dominant sources, as well as in western England and Northern Ireland, particularly in July,
 431 where dairy cattle farming dominates (Hellsten et al., 2008). The spatial correlation between top-
 432 down and bottom-up gridded emissions in general ranges from $R = 0.5$ to $R = 0.7$, except for
 433 IASI in September ($R = 0.34$) when dynamic range in emissions is low.

434 The bottom-up emissions for March-September total 198.7 Gg. This is 27% less than
 435 IASI and 49% less than CrIS. According to the bottom-up inventory and Hellsten et al. (2007),
 436 March-September captures 60-67% of annual emissions. If we use this to scale IASI and CrIS to

437 annual totals, this suggests annual NH₃ emissions of 405-453 Gg according to IASI and 581-649
 438 Gg according to CrIS. Natural NH₃ emissions total ~22 Gg in the UK (Section 3), so top-down
 439 annual anthropogenic NH₃ emissions are 383-431 Gg according to IASI and 559-627 Gg
 440 according to CrIS. Both top-down estimates exceed annual total anthropogenic emissions from
 441 the NAEI of 276 Gg (Section 3) and the UNECE Gothenburg emissions ceiling of 297 Gg.

442



443

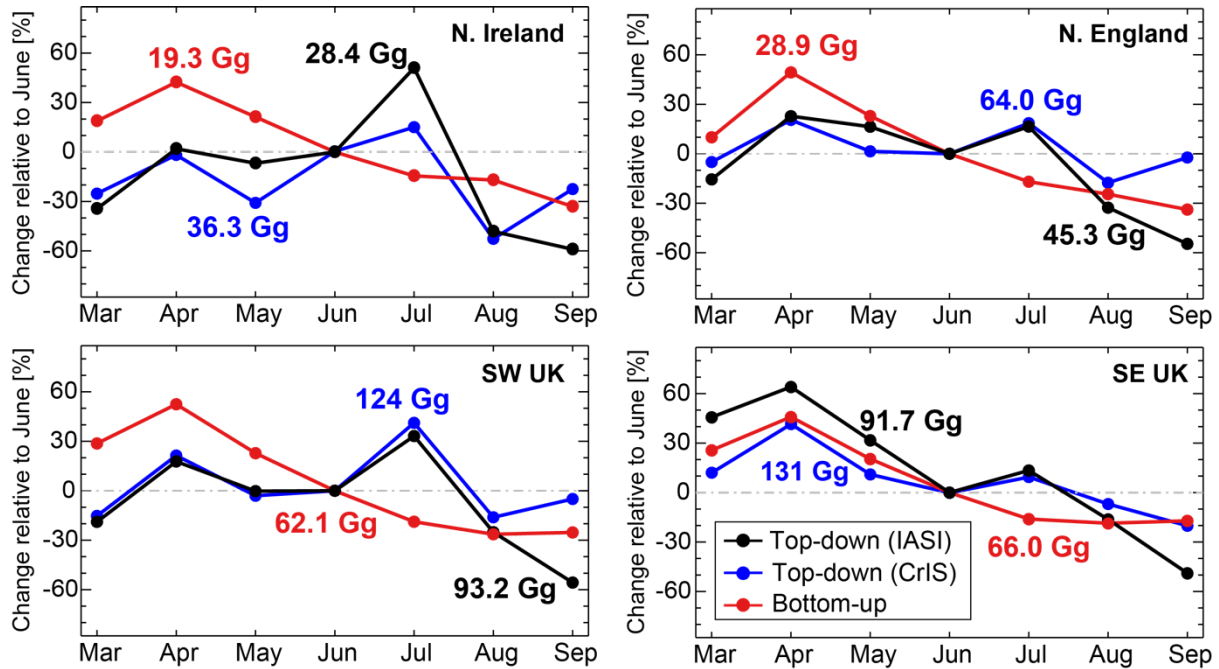
444

445 **Figure 6.** Comparison of bottom-up and top-down NH₃ emissions for April and July. Panels are
 446 bottom-up emissions (left), and the difference between top-down and bottom-up emissions for
 447 IASI (middle) and CrIS (right) in April (top row) and July (bottom row). Grids are blue for
 448 bottom-up < top-down and red for bottom-up > top-down. Values inset are bottom-up total (left)
 449 and differences in (middle and right) monthly emissions and the Pearson's spatial correlation (*R*)
 450 between top-down and bottom-up emissions.

451 Figure 7 compares regional seasonality in UK NH₃ emissions from bottom-up and top-
 452 down estimates as the percent change in monthly means relative to June. Regional seasonality in
 453 the top-down emissions is very similar in March-August in all regions except Northern Ireland.
 454 The mismatch between IASI and CrIS in September is due to a positive offset in CrIS relative to
 455 IASI columns. The July peak in emissions in Northern Ireland is more pronounced in IASI than
 456 CrIS. This is also apparent in the seasonality in the column densities (Figure S4). This may be
 457 due to differences in temporal coverage of the two sensors (2008-2018 for IASI, 2013-2018 for
 458 CrIS) over a location that has experienced dramatic changes in agricultural activity. This
 459 includes increases in livestock numbers of 45% for pigs and 42% for table chickens and a decline
 460 in nitrogen fertilizer of 37% from 2000 to 2016 (DEFRA, 2020b). All emission estimates exhibit
 461 a spring peak in April due to intensive fertilizer and manure application in March-April (Hellsten

462 et al., 2007). Paulot et al. (2014) also identified this April peak in NH₃ emissions inferred from
 463 ammonium wet deposition measurements, though a recent study questions the utility of these
 464 measurements for constraining NH₃ emissions (Tan et al., 2020). A second summer peak in the
 465 top-down emissions in July that is not present in the bottom-up inventory could be due to manure
 466 spreading and dairy farming (Hellsten et al., 2007). The likely contribution from dairy farming is
 467 supported by spatial consistency between the July top-down emissions (Figures 4 and 5) and
 468 locations dominated by emissions from dairy cattle (Hellsten et al., 2008).

469



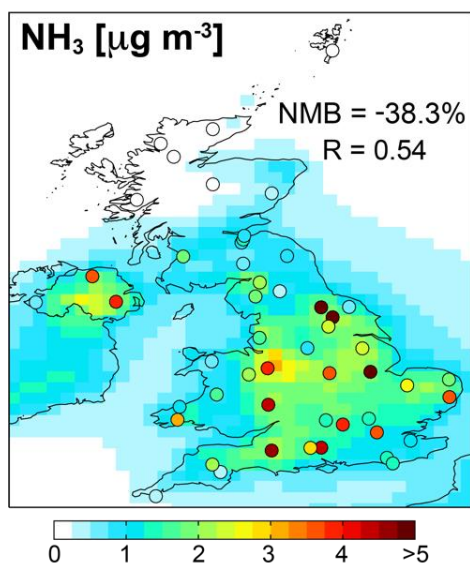
470

471

472 **Figure 7.** Regional seasonality in March-September NH₃ emissions. Points are the percentage
 473 change in monthly emissions relative to June for top-down emissions from IASI (black) and CrIS
 474 (blue), and from the bottom-up inventory (red). Regions sampled are in Figure 3. Inset values are
 475 March-September totals for each region from each estimate.

476 In Figure 8, we compare March-September 2016 mean modelled and observed surface
 477 concentrations of NH_3 to determine if the model driven with NAEI NH_3 emissions and prior
 478 assumptions of NH_3 seasonality and diurnal variability corroborates the results obtained with the
 479 satellite observations. Monthly means from model grids coincident with the surface sites are
 480 reasonably spatially consistent with the surface observations ($R = 0.54$) and the model is 38.3%
 481 less than the observations. This is midway between the NAEI comparison to the top-down
 482 emissions of 27% less than IASI and 49% less than CrIS. There are also rural low-cost passive
 483 sampler measurements of NH_3 concentrations, but these have low precision and are only reliable
 484 (within $\pm 10\%$ of reference measurements) at $\text{NH}_3 \geq 2 \mu\text{g m}^{-3}$ (Martin et al., 2019; Sutton et al.,
 485 2001). Even so, the model is similarly biased low (by 41.5%) compared to these measurements
 486 (not shown).

487



488

489

490 **Figure 8.** Comparison of observed and modelled surface concentrations of NH_3 . Data are EMEP
 491 and UKEAP site measurements (points) and the model (background) for March-September 2016.
 492 Inset values are the Pearson's spatio-temporal correlation coefficient (R) and the model NMB for
 493 coincident monthly means.

494 **6 Error analysis of the top-down emissions**

495 The reported relative error for NAEI NH_3 emissions is 31% (Ricardo, 2018a).
 496 Quantifiable random errors that contribute to total March-September satellite-derived emissions
 497 include uncertainties in retrieval of NH_3 , and in the modelled relationship between NH_3
 498 emissions and column densities. For the latter we test sensitivity to modelled sulfate aerosol and
 499 nitric acid abundances and prior assumptions of the spatial and temporal variability of NH_3
 500 emissions. IASI NH_3 retrieval errors for columns $\geq 2 \times 10^{15}$ molecules cm^{-2} range from 0.7-
 501 34%. Retrieval errors larger than 34% do occur, but are in locations with very low emissions.
 502 The CrIS NH_3 column errors across all grids range from 0.2-25%. Error contributions from
 503 uncertainties in sulfate and nitric acid are small compared to column density retrievals. We
 504 estimate these as the change in top-down emissions due to a perturbation in SO_2 emissions for

505 sulfate and NO_x emissions for nitric acid. The percent change in top-down emissions from a 50%
506 decrease in SO_2 emissions is 4-5%. A 50% increase in NO_x emissions increases nitric acid by
507 14%, aerosol nitrate by 11%, and satellite-derived NH_3 emissions by 8-9%. The limited
508 sensitivity to sulfate and nitrate in the UK is because NH_3 is in excess due to the success of
509 emission controls targeting SO_2 and NO_x sources and absence of these for NH_3 sources. We also
510 find that our top-down emissions estimates are relatively insensitive to NH_3 emissions
511 perturbations. A 50% increase in NH_3 emissions causes a small (3%) decrease in satellite-derived
512 NH_3 emissions. The total relative error from adding these individual errors in quadrature is 11-
513 36% for IASI and 9-27% for CrIS and is dominated by errors in retrieval of the columns. Total
514 emissions for March-September are 198.7 ± 61.6 Gg for the bottom-up inventory and up to 271.5
515 ± 97.7 Gg for IASI and 389.6 ± 105.2 Gg for CrIS.

516 There are also known systematic biases. Some studies reported that IASI NH_3 column
517 densities are biased low by 25-50% compared to ground-based measurements (Dammers et al.,
518 2017; Whitburn et al., 2016a). However, these comparisons were for earlier versions of the IASI
519 NH_3 product. The version used here is consistent with columns derived with aircraft observations
520 (Guo et al., 2021), though Guo et al. (2021) caution that their comparison is limited in time
521 (summer) and location (Colorado, US) and sensitive to errors in column estimates from
522 integrating aircraft measurements. The CrIS column amounts display a gradual increase with
523 time (Figure S1) that we correct for in this work, though further work is required to determine
524 the cause. Both satellite products preferentially sample clear-sky conditions. The bias that this
525 may cause is challenging to quantify. Warmer temperatures and absence of clouds would reduce
526 the amount of NH_3 that partitions to the aqueous phase (Stelson & Seinfeld, 1982; Walters et al.,
527 2018), but NH_3 emissions would also increase (Sutton et al., 2013). The largest impact of clear-
528 sky sampling in the UK may be in July, when boundary-layer clear-sky air temperatures,
529 according to GEOS-Chem, are $\sim 6^\circ\text{C}$ warmer than all-sky scenes.

530 **5 Conclusions**

531 Emissions of ammonia (NH_3) in the UK are mostly (>80%) from agriculture and are
532 challenging to estimate with bottom-up approaches and validate exclusively with current ground-
533 based networks. Here we used satellite observations of NH_3 in March-September for multiple
534 years from the Infrared Atmospheric Sounding Interferometer (IASI) (2008-2018) and the Cross-
535 track Infrared Sounder (CrIS) (2013-2018) with the GEOS-Chem chemical transport model to
536 derive top-down monthly emissions across the UK at high spatial resolution (~ 10 km).

537 Total top-down March-September emissions are 272 Gg from IASI and 390 Gg from
538 CrIS. Bottom-up emissions estimated with the UK National Atmospheric Emission Inventory
539 (NAEI) annual emissions and GEOS-Chem monthly scaling factors are 27% less than IASI-
540 derived emissions and 49% less than CrIS-derived emissions. This is supported by a 38-42%
541 underestimate in surface NH_3 concentrations from GEOS-Chem driven with the NAEI. We infer
542 UK top-down annual anthropogenic NH_3 emissions of 383-431 Gg from IASI and 559-627 Gg
543 from CrIS compared to 276 Gg from the NAEI. Seasonality in the top-down emissions confirms
544 the well-known spring April peak from fertilizer and manure use, but there is also a summer July
545 peak coincident with intensive dairy farming that is absent in the bottom-up inventory.

546 The relative error in the top-down emissions, mostly due to NH₃ column retrieval errors,
 547 is 11-36% for IASI and 9-27% for CrIS and is similar to the error reported for the NAEI (31%).
 548 The top-down emissions estimates are relatively insensitive to model uncertainties in SO₂, NO_x
 549 and NH₃ emissions, as NH₃ is in excess and the relationship between modelled NH₃ columns and
 550 emissions is near-linear.

551 Our study demonstrates the tremendous potential to use satellite observations to derive
 552 NH₃ emissions and assess bottom-up inventories under particularly challenging observing
 553 conditions (cloudy, cool) in the UK. This is critical for assessing reliability of these inventories
 554 for informing policies and mitigation strategies. The discrepancy between bottom-up and top-
 555 down emissions identified here warrants further investigation of both approaches.

556 **Acknowledgments, Samples, and Data**

557 The authors are grateful for helpful discussions with Daven Henze and Hansen Cao. EAM and
 558 AKP acknowledge funding from DEFRA (contract reference ecm_55415) and EAM
 559 acknowledges additional funding from NERC/EPSRC (grant number EP/R513465/1). The
 560 research in Belgium was funded by the F.R.S.-FNRS and the Belgian State Federal Office for
 561 Scientific, Technical and Cultural Affairs (Prodex 645 arrangement IASI.FLOW). Both MVD
 562 and LC are supported by the Belgian F.R.S.-FNRS.

563 The top-down and bottom-up emissions estimated in this work are publicly available from the
 564 UCL Data Repository (<https://doi.org/10.5522/04/14566635>). The CrIS CFPR NH₃ data are
 565 created by Environment and Climate Change Canada and hosted by the Meteorological Service
 566 of Canada (MSC) Datamart. Access to the CrIS NH₃ data can be requested from MWS
 567 (mark.shephard@canada.ca). The IASI NH₃ data are publicly available from the IASI data
 568 catalogue (<https://iasi.aeris-data.fr/nh3/>).
 569

570 **References**

- 571 Adams, C., McLinden, C. A., Shephard, M. W., Dickson, N., Dammers, E., Chen, J., et al.
 572 (2019), Satellite-derived emissions of carbon monoxide, ammonia, and nitrogen dioxide from the
 573 2016 Horse River wildfire in the Fort McMurray area, *Atmospheric Chemistry and Physics*,
 574 *19*(4), 2577-2599, doi:10.5194/acp-19-2577-2019.
 575 AIC (2020). *B2.4 Total quantities of nitrogen, phosphate and potash, UK*. Retrieved from
 576 [https://www.agindustries.org.uk/static/0dd85abd-807d-4137-a00e609888633c89/Fertiliser-](https://www.agindustries.org.uk/static/0dd85abd-807d-4137-a00e609888633c89/Fertiliser-consumption-in-the-UK-quantity-data.pdf)
 577 [consumption-in-the-UK-quantity-data.pdf](https://www.agindustries.org.uk/static/0dd85abd-807d-4137-a00e609888633c89/Fertiliser-consumption-in-the-UK-quantity-data.pdf)
 578 Amos, H. M., Jacob, D. J., Holmes, C. D., Fisher, J. A., Wang, Q., Yantosca, R. M., et al. (2012),
 579 Gas-particle partitioning of atmospheric Hg(II) and its effect on global mercury deposition,
 580 *Atmospheric Chemistry and Physics*, *12*(1), 591-603, doi:10.5194/acp-12-591-2012.
 581 Beer, R., Shephard, M. W., Kulawik, S. S., Clough, S. A., Eldering, A., Bowman, K. W., et al.
 582 (2008), First satellite observations of lower tropospheric ammonia and methanol, *Geophysical*
 583 *Research Letters*, *35*(9), L09801, doi:10.1029/2008gl033642.
 584 BEIS (2016). *Offshore Energy Energy Strategic Environmental Assessment 3 (OESEA3)*
 585 *Appendix 1*. Retrieved from
 586 [https://assets.publishing.service.gov.uk/government/uploads/system/uploads/attachment_data/file](https://assets.publishing.service.gov.uk/government/uploads/system/uploads/attachment_data/file/504559/OESEA3_A1f_Climate_Meteorology.pdf)
 587 [/504559/OESEA3_A1f_Climate_Meteorology.pdf](https://assets.publishing.service.gov.uk/government/uploads/system/uploads/attachment_data/file/504559/OESEA3_A1f_Climate_Meteorology.pdf)

- 588 Boersma, A., Pels, J., Cieplik, M., van der Linden, R., Hesselings, W., & Heslinga, D. (2008).
589 *Emissions of the use of biomass fuels in stationary applications* Retrieved from
590 https://www.rivm.nl/bibliotheek/digitaaldepot/BOLK_I_biomass_Final.pdf
- 591 Bouwman, A. F., Lee, D. S., Asman, W. A. H., Dentener, F. J., VanderHoek, K. W., & Olivier,
592 J. G. J. (1997), A global high-resolution emission inventory for ammonia, *Global*
593 *Biogeochemical Cycles*, *11*(4), 561-587, doi:10.1029/97gb02266.
- 594 Cady-Pereira, K. E., Payne, V. H., Neu, J. L., Bowman, K. W., Miyazaki, K., Marais, E. A., et al.
595 (2017), Seasonal and spatial changes in trace gases over megacities from Aura TES observations:
596 two case studies, *Atmospheric Chemistry and Physics*, *17*(15), 9379-9398, doi:10.5194/acp-17-
597 9379-2017.
- 598 Chen, Y., Shen, H., Kaiser, J., Hu, Y., Capps, S. L., Zhao, S., et al. (2021), High-resolution
599 hybrid inversion of IASI ammonia columns to constrain US ammonia emissions using the
600 CMAQ adjoint model, *Atmospheric Chemistry and Physics*, *21*(3), 2067-2082, doi:10.5194/acp-
601 21-2067-2021.
- 602 Chin, M., Savoie, D. L., Huebert, B. J., Bandy, A. R., Thornton, D. C., Bates, T. S., et al. (2000),
603 Atmospheric sulfur cycle simulated in the global model GOCART: Comparison with field
604 observations and regional budgets, *Journal of Geophysical Research: Atmospheres*, *105*(D20),
605 24689-24712, doi:10.1029/2000jd900385.
- 606 Clarisse, L., Clerbaux, C., Dentener, F., Hurtmans, D., & Coheur, P.-F. (2009), Global ammonia
607 distribution derived from infrared satellite observations, *Nature Geoscience*, *2*(7), 479-483,
608 doi:10.1038/ngeo551.
- 609 Clarisse, L., Shephard, M. W., Dentener, F., Hurtmans, D., Cady-Pereira, K., Karagulian, F., et
610 al. (2010), Satellite monitoring of ammonia: A case study of the San Joaquin Valley, *Journal of*
611 *Geophysical Research: Atmospheres*, *115*(D13), D13302, doi:10.1029/2009jd013291.
- 612 Clarisse, L., R'Honi, Y., Coheur, P.-F., Hurtmans, D., & Clerbaux, C. (2011), Thermal infrared
613 nadir observations of 24 atmospheric gases, *Geophysical Research Letters*, *38*(10), L10802,
614 doi:10.1029/2011gl047271.
- 615 Clarisse, L., Van Damme, M., Clerbaux, C., & Coheur, P. F. (2019), Tracking down global NH₃
616 point sources with wind-adjusted superresolution, *Atmospheric Measurement Techniques*,
617 *12*(10), 5457-5473, doi:10.5194/amt-12-5457-2019.
- 618 Cohen, A. J., Brauer, M., Burnett, R., Anderson, H. R., Frostad, J., Estep, K., et al. (2017),
619 Estimates and 25-year trends of the global burden of disease attributable to ambient air pollution:
620 an analysis of data from the Global Burden of Diseases Study 2015, *The Lancet*, *389*(10082),
621 1907-1918, doi:10.1016/s0140-6736(17)30505-6.
- 622 Dammers, E., Palm, M., Van Damme, M., Vigouroux, C., Smale, D., Conway, S., et al. (2016),
623 An evaluation of IASI-NH₃ with ground-based Fourier transform infrared spectroscopy
624 measurements, *Atmospheric Chemistry and Physics*, *16*(16), 10351-10368, doi:10.5194/acp-16-
625 10351-2016.
- 626 Dammers, E., Shephard, M. W., Palm, M., Cady-Pereira, K., Capps, S., Lutsch, E., et al. (2017),
627 Validation of the CrIS fast physical NH₃ retrieval with ground-based FTIR, *Atmospheric*
628 *Measurement Techniques*, *10*(7), 2645-2667, doi:10.5194/amt-10-2645-2017.
- 629 Dammers, E., McLinden, C. A., Griffin, D., Shephard, M. W., Van der Graaf, S., Lutsch, E., et
630 al. (2019), NH₃ emissions from large point sources derived from CrIS and IASI satellite
631 observations, *Atmospheric Chemistry and Physics*, *19*(19), 12261-12293, doi:10.5194/acp-19-
632 12261-2019.

- 633 DEFRA (2016a). *Maps of livestock populations in 2000 and 2010 across England*. Retrieved
634 from
635 https://assets.publishing.service.gov.uk/government/uploads/system/uploads/attachment_data/file/183109/defra-stats-foodfarm-landuselivestock-june-detailedresults-livestockmaps111125.pdf
636
637 DEFRA (2016b). *Maps of crop areas in 2000 and 2010 across England*. Retrieved from
638 https://assets.publishing.service.gov.uk/government/uploads/system/uploads/attachment_data/file/183108/defra-stats-foodfarm-landuselivestock-june-detailedresults-cropmaps111125.pdf
639
640 DEFRA (2019). *Clean Air Strategy 2019*. Retrieved from
641 <https://www.gov.uk/government/publications/clean-air-strategy-2019>
642 DEFRA (2020a). *Consultation on reducing ammonia emissions from solid urea fertilisers*.
643 Retrieved from [https://consult.defra.gov.uk/air-quality-and-industrial-emissions/reducing-](https://consult.defra.gov.uk/air-quality-and-industrial-emissions/reducing-ammonia-emissions-from-urea-fertilisers/supporting_documents/Solid%20Urea%20Fertilisers%20Consultation%20Document%20Nov%202020.pdf)
644 [ammonia-emissions-from-urea-](https://consult.defra.gov.uk/air-quality-and-industrial-emissions/reducing-ammonia-emissions-from-urea-fertilisers/supporting_documents/Solid%20Urea%20Fertilisers%20Consultation%20Document%20Nov%202020.pdf)
645 [fertilisers/supporting_documents/Solid%20Urea%20Fertilisers%20Consultation%20Document](https://consult.defra.gov.uk/air-quality-and-industrial-emissions/reducing-ammonia-emissions-from-urea-fertilisers/supporting_documents/Solid%20Urea%20Fertilisers%20Consultation%20Document%20Nov%202020.pdf)
646 [Nov%202020.pdf](https://consult.defra.gov.uk/air-quality-and-industrial-emissions/reducing-ammonia-emissions-from-urea-fertilisers/supporting_documents/Solid%20Urea%20Fertilisers%20Consultation%20Document%20Nov%202020.pdf)
647 DEFRA (2020b). *Key crop areas and livestock numbers: UK and country level data 1866-2020*.
648 Retrieved from
649 https://assets.publishing.service.gov.uk/government/uploads/system/uploads/attachment_data/file/946207/structure-june-ukkeyresults-22dec20.ods. Accessed on 5 January 2021.
650
651 Dockery, D. W., Pope, C. A., Xu, X., Spengler, J. D., Ware, J. H., Fay, M. E., et al. (1993), An
652 association between air pollution and mortality in six U.S. cities, *New England Journal of*
653 *Medicine*, 329(24), 1753-1759, doi:10.1056/nejm199312093292401.
654 Fortems-Cheiney, A., Dufour, G., Dufossé, K., Couvidat, F., Gilliot, J.-M., Siour, G., et al.
655 (2020), Do alternative inventories converge on the spatiotemporal representation of spring
656 ammonia emissions in France?, *Atmospheric Chemistry and Physics*, 20(21), 13481-13495,
657 doi:10.5194/acp-20-13481-2020.
658 Fountoukis, C., & Nenes, A. (2007), ISORROPIA II: a computationally efficient thermodynamic
659 equilibrium model for K^+ - Ca^{2+} - Mg^{2+} - NH_4^+ - Na^+ - SO_4^{2-} - NO_3^- - Cl^- - H_2O aerosols, *Atmospheric*
660 *Chemistry and Physics*, 7(17), 4639-4659, doi:10.5194/acp-7-4639-2007.
661 Friedrich, R. (2000), GENEMIS: Generation of European Emission Data for Episodes, in
662 *Transport and Chemical Transformation of Pollutants in the Troposphere*, edited by P. Borrell,
663 Borrell, P. M. & Midgley, P., pp. 375-386, Springer-Verlag, Berlin, doi:10.1007/978-3-642-
664 59718-3_18.
665 Galloway, J. N. (1998), The global nitrogen cycle: changes and consequences, *Environmental*
666 *Pollution*, 102(1), 15-24, doi:10.1016/s0269-7491(98)80010-9.
667 Goldberg, M. D., Kilcoyne, H., Cikanek, H., & Mehta, A. (2013), Joint Polar Satellite System:
668 The United States next generation civilian polar-orbiting environmental satellite system, *Journal*
669 *of Geophysical Research: Atmospheres*, 118(24), 13463-13475, doi:10.1002/2013jd020389.
670 Guo, X., Clarisse, L., Wang, R., Van Damme, M., Whitburn, S., Coheur, P. F., et al. (2021),
671 Validation of IASI satellite ammonia observations at the pixel scale using in-situ vertical
672 profiles, *Journal of Geophysical Research: Atmospheres*, 126, doi:10.1029/2020jd033475.
673 Hauglustaine, D. A., Balkanski, Y., & Schulz, M. (2014), A global model simulation of present
674 and future nitrate aerosols and their direct radiative forcing of climate, *Atmospheric Chemistry*
675 *and Physics*, 14(20), 11031-11063, doi:10.5194/acp-14-11031-2014.
676 Heald, C. L., Collett, J. L., Lee, T., Benedict, K. B., Schwandner, F. M., Li, Y., et al. (2012),
677 Atmospheric ammonia and particulate inorganic nitrogen over the United States, *Atmospheric*
678 *Chemistry and Physics*, 12(21), 10295-10312, doi:10.5194/acp-12-10295-2012.

- 679 Hellsten, S., Dragosits, U., Place, C. J., Misselbrook, T. H., Tang, Y. S., & Sutton, M. A. (2007),
680 Modelling seasonal dynamics from temporal variation in agricultural practices in the UK
681 ammonia emission inventory, *Water, Air, & Soil Pollution: Focus*, 7(1-3), 3-13,
682 doi:10.1007/s11267-006-9087-5.
- 683 Hellsten, S., Dragosits, U., Place, C. J., Vieno, M., Dore, A. J., Misselbrook, T. H., et al. (2008),
684 Modelling the spatial distribution of ammonia emissions in the UK, *Environmental Pollution*,
685 154(3), 370-379, doi:10.1016/j.envpol.2008.02.017.
- 686 Hickman, J. E., Dammers, E., Galy-Lacaux, C., & van der Werf, G. R. (2018), Satellite evidence
687 of substantial rain-induced soil emissions of ammonia across the Sahel, *Atmospheric Chemistry
688 and Physics*, 18(22), 16713-16727, doi:10.5194/acp-18-16713-2018.
- 689 Hickman, J. E., Andela, N., Dammers, E., Clarisse, L., Coheur, P.-F., Van Damme, M., et al.
690 (2020), Changes in biomass burning, wetland extent, or agriculture drive atmospheric NH₃ trends
691 in several African regions, *Atmospheric Chemistry and Physics Discussions*, doi:10.5194/acp-
692 2020-945.
- 693 Johnson, P. T. J., & Carpenter, S. R. (2010), Chapter Four. Influence of Eutrophication on
694 Disease in Aquatic Ecosystems: Patterns, Processes, and Predictions, in *Infectious Disease
695 Ecology*, edited by R. S. Ostfeld, Keesing, F. & Eviner, V. T., pp. 71-99, Princeton University
696 Press, Princeton, NJ, doi:10.1515/9781400837885.71.
- 697 Keller, C. A., Long, M. S., Yantosca, R. M., Da Silva, A. M., Pawson, S., & Jacob, D. J. (2014),
698 HEMCO v1.0: a versatile, ESMF-compliant component for calculating emissions in atmospheric
699 models, *Geoscientific Model Development*, 7(4), 1409-1417, doi:10.5194/gmd-7-1409-2014.
- 700 Luo, G., Yu, F. Q., & Schwab, J. (2019), Revised treatment of wet scavenging processes
701 dramatically improves GEOS-Chem 12.0.0 simulations of surface nitric acid, nitrate, and
702 ammonium over the United States, *Geoscientific Model Development*, 12(8), 3439-3447,
703 doi:10.5194/gmd-12-3439-2019.
- 704 Luo, G., Yu, F., & Moch, J. M. (2020), Further improvement of wet process treatments in
705 GEOS-Chem v12.6.0: impact on global distributions of aerosols and aerosol precursors,
706 *Geoscientific Model Development*, 13(6), 2879-2903, doi:10.5194/gmd-13-2879-2020.
- 707 Makkonen, U., Virkkula, A., Mantykentta, J., Hakola, H., Keronen, P., Vakkari, V., & Aalto, P.
708 P. (2012), Semi-continuous gas and inorganic aerosol measurements at a Finnish urban site:
709 comparisons with filters, nitrogen in aerosol and gas phases, and aerosol acidity, *Atmospheric
710 Chemistry and Physics*, 12(12), 5617-5631, doi:10.5194/acp-12-5617-2012.
- 711 Marais, E. A., Jacob, D. J., Kurosu, T. P., Chance, K., Murphy, J. G., Reeves, C., et al. (2012),
712 Isoprene emissions in Africa inferred from OMI observations of formaldehyde columns,
713 *Atmospheric Chemistry and Physics*, 12(14), 6219-6235, doi:10.5194/acp-12-6219-2012.
- 714 Martin, N. A., Ferracci, V., Cassidy, N., Hook, J., Battersby, R. M., di Meane, E. A., et al.
715 (2019), Validation of ammonia diffusive and pumped samplers in a controlled atmosphere test
716 facility using traceable Primary Standard Gas Mixtures, *Atmospheric Environment*, 199, 453-
717 462, doi:10.1016/j.atmosenv.2018.11.038.
- 718 McCarthy, M., Christidis, N., Dunstone, N., Fereday, D., Kay, G., Klein-Tank, A., et al. (2019),
719 Drivers of the UK summer heatwave of 2018, *Weather*, 74(11), 390-396, doi:10.1002/wea.3628.
- 720 Misselbrook, T. H., Sutton, M. A., & Scholefield, D. (2006), A simple process-based model for
721 estimating ammonia emissions from agricultural land after fertilizer applications, *Soil Use and
722 Management*, 20(4), 365-372, doi:10.1111/j.1475-2743.2004.tb00385.x.

- 723 Nowak, J. B., Neuman, J. A., Bahreini, R., Brock, C. A., Middlebrook, A. M., Wollny, A. G., et
724 al. (2010), Airborne observations of ammonia and ammonium nitrate formation over Houston,
725 Texas, *Journal of Geophysical Research*, *115*(D22), D22304, doi:10.1029/2010jd014195.
- 726 Palmer, P. I., Jacob, D. J., Fiore, A. M., Martin, R. V., Chance, K., & Kurosu, T. P. (2003),
727 Mapping isoprene emissions over North America using formaldehyde column observations from
728 space, *Journal of Geophysical Research: Atmospheres*, *108*(D6), 4180,
729 doi:10.1029/2002jd002153.
- 730 Park, R. J., Jacob, D. J., Field, B. D., Yantosca, R. M., & Chin, M. (2004), Natural and
731 transboundary pollution influences on sulfate-nitrate-ammonium aerosols in the United States:
732 Implications for policy, *Journal of Geophysical Research: Atmospheres*, *109*(D15), D15204,
733 doi:10.1029/2003jd004473.
- 734 Paulot, F., Jacob, D. J., Pinder, R. W., Bash, J. O., Travis, K., & Henze, D. K. (2014), Ammonia
735 emissions in the United States, European Union, and China derived by high-resolution inversion
736 of ammonium wet deposition data: Interpretation with a new agricultural emissions inventory
737 (MASAGE_NH3), *Journal of Geophysical Research: Atmospheres*, *119*(7), 4343-4364,
738 doi:10.1002/2013jd021130.
- 739 Paulrud, S., Kindbom, K., & Gustafsson, T. (2006). *Emission factors and emissions from*
740 *residential biomass combustion in Sweden*. Retrieved from [https://www.diva-](https://www.diva-portal.org/smash/get/diva2:1184181/FULLTEXT01.pdf)
741 [portal.org/smash/get/diva2:1184181/FULLTEXT01.pdf](https://www.diva-portal.org/smash/get/diva2:1184181/FULLTEXT01.pdf)
- 742 Ricardo (2017). *A review of the NAEI shipping emissions methodology: Final report*. Retrieved
743 from [https://uk-](https://uk-air.defra.gov.uk/assets/documents/reports/cat07/1712140936_ED61406_NAEI_shipping_report_12Dec2017.pdf)
744 [air.defra.gov.uk/assets/documents/reports/cat07/1712140936_ED61406_NAEI_shipping_report_](https://uk-air.defra.gov.uk/assets/documents/reports/cat07/1712140936_ED61406_NAEI_shipping_report_12Dec2017.pdf)
745 [12Dec2017.pdf](https://uk-air.defra.gov.uk/assets/documents/reports/cat07/1712140936_ED61406_NAEI_shipping_report_12Dec2017.pdf)
- 746 Ricardo (2018a). *UK Informative Inventory Report (1990 to 2016)*. Retrieved from [https://uk-](https://uk-air.defra.gov.uk/assets/documents/reports/cat07/1803161032_GB_IIR_2018_v1.2.pdf)
747 [air.defra.gov.uk/assets/documents/reports/cat07/1803161032_GB_IIR_2018_v1.2.pdf](https://uk-air.defra.gov.uk/assets/documents/reports/cat07/1803161032_GB_IIR_2018_v1.2.pdf)
- 748 Ricardo (2018b). *UK Emission Mapping Methodology: A report of the National Atmospheric*
749 *Emission Inventory 2016*. Retrieved from [https://uk-](https://uk-air.defra.gov.uk/assets/documents/reports/cat07/1812061112_MappingMethodology-for-NAEI-2016.pdf)
750 [air.defra.gov.uk/assets/documents/reports/cat07/1812061112_MappingMethodology-for-NAEI-](https://uk-air.defra.gov.uk/assets/documents/reports/cat07/1812061112_MappingMethodology-for-NAEI-2016.pdf)
751 [2016.pdf](https://uk-air.defra.gov.uk/assets/documents/reports/cat07/1812061112_MappingMethodology-for-NAEI-2016.pdf)
- 752 Ricardo (2019a). *UK Informative Inventory Report (1990 to 2017)*. Retrieved from [https://uk-](https://uk-air.defra.gov.uk/assets/documents/reports/cat09/1904121008_GB_IIR_2019_v2.0.pdf)
753 [air.defra.gov.uk/assets/documents/reports/cat09/1904121008_GB_IIR_2019_v2.0.pdf](https://uk-air.defra.gov.uk/assets/documents/reports/cat09/1904121008_GB_IIR_2019_v2.0.pdf)
- 754 Ricardo (2019b). *Ammonia futures: understanding implications for habitats and requirements*
755 *for uptake of mitigation measures*. Retrieved from [https://uk-](https://uk-air.defra.gov.uk/assets/documents/reports/cat09/1909040930_Ammonia_futures_Understanding_implications_for_habitats_requirements_for_uptake_of_mitigation_measures_Modelling_workshop_report.pdf)
756 [air.defra.gov.uk/assets/documents/reports/cat09/1909040930_Ammonia_futures_Understanding](https://uk-air.defra.gov.uk/assets/documents/reports/cat09/1909040930_Ammonia_futures_Understanding_implications_for_habitats_requirements_for_uptake_of_mitigation_measures_Modelling_workshop_report.pdf)
757 [_implications_for_habitats_requirements_for_uptake_of_mitigation_measures Modelling work](https://uk-air.defra.gov.uk/assets/documents/reports/cat09/1909040930_Ammonia_futures_Understanding_implications_for_habitats_requirements_for_uptake_of_mitigation_measures_Modelling_workshop_report.pdf)
758 [shop_report.pdf](https://uk-air.defra.gov.uk/assets/documents/reports/cat09/1909040930_Ammonia_futures_Understanding_implications_for_habitats_requirements_for_uptake_of_mitigation_measures_Modelling_workshop_report.pdf)
- 759 Ricardo (2020). *UK Informative Inventory Report (1990 to 2018)*. Retrieved from [https://uk-](https://uk-air.defra.gov.uk/assets/documents/reports/cat07/2003131327_GB_IIR_2020_v1.0.pdf)
760 [air.defra.gov.uk/assets/documents/reports/cat07/2003131327_GB_IIR_2020_v1.0.pdf](https://uk-air.defra.gov.uk/assets/documents/reports/cat07/2003131327_GB_IIR_2020_v1.0.pdf)
- 761 Riddick, S. N., Dragosits, U., Blackall, T. D., Daunt, F., Wanless, S., & Sutton, M. A. (2012),
762 The global distribution of ammonia emissions from seabird colonies, *Atmospheric Environment*,
763 *55*, 319-327, doi:10.1016/j.atmosenv.2012.02.052.
- 764 Rodgers (2000), *Inverse Methods for Atmospheric Sounding - Theory and Practice*, World
765 Scientific, River Edge, N.J., doi:10.1142/3171.
- 766 Schiferl, L. D., Heald, C. L., Van Damme, M., Clarisse, L., Clerbaux, C., Coheur, P.-F., et al.
767 (2016), Interannual variability of ammonia concentrations over the United States: sources and

- 768 implications, *Atmospheric Chemistry and Physics*, 16(18), 12305-12328, doi:10.5194/acp-16-
769 12305-2016.
- 770 Shephard, M. W., Cady-Pereira, K. E., Luo, M., Henze, D. K., Pinder, R. W., Walker, J. T., et al.
771 (2011), TES ammonia retrieval strategy and global observations of the spatial and seasonal
772 variability of ammonia, *Atmospheric Chemistry and Physics*, 11(20), 10743-10763,
773 doi:10.5194/acp-11-10743-2011.
- 774 Shephard, M. W., & Cady-Pereira, K. E. (2015), Cross-track Infrared Sounder (CrIS) satellite
775 observations of tropospheric ammonia, *Atmospheric Measurement Techniques*, 8(3), 1323-1336,
776 doi:10.5194/amt-8-1323-2015.
- 777 Shephard, M. W., Dammers, E., Cady-Pereira, K. E., Kharol, S. K., Thompson, J., Gainariu-
778 Matz, Y., et al. (2020), Ammonia measurements from space with the Cross-track Infrared
779 Sounder: characteristics and applications, *Atmospheric Chemistry and Physics*, 20(4), 2277-
780 2302, doi:10.5194/acp-20-2277-2020.
- 781 Simet, A. (2017). *Drax reports good operational year, discusses future in biomass*. Retrieved
782 from [http://biomassmagazine.com/articles/14201/drax-reports-good-operational-year-discusses-
783 future-in-biomass](http://biomassmagazine.com/articles/14201/drax-reports-good-operational-year-discusses-future-in-biomass)
- 784 Simpson, D., Winiwarter, W., Borjesson, G., Cinderby, S., Ferreiro, A., Guenther, A., et al.
785 (1999), Inventorying emissions from nature in Europe, *Journal of Geophysical Research:
786 Atmospheres*, 104(D7), 8113-8152, doi:10.1029/98JD02747.
- 787 Stelson, A. W., & Seinfeld, J. H. (1982), Relative humidity and temperature dependence of the
788 ammonium nitrate dissociation constant, *Atmospheric Environment*, 16(5), 983-992,
789 doi:10.1016/0004-6981(82)90184-6.
- 790 Stettler, M. E. J., Eastham, S., & Barrett, S. R. H. (2011), Air quality and public health impacts
791 of UK airports. Part I: Emissions, *Atmospheric Environment*, 45(31), 5415-5424,
792 doi:10.1016/j.atmosenv.2011.07.012.
- 793 Stieger, B., Spindler, G., Fahlbusch, B., Müller, K., Grüner, A., Poulain, L., et al. (2017),
794 Measurements of PM₁₀ ions and trace gases with the online system MARGA at the research
795 station Melpitz in Germany – A five-year study, *Journal of Atmospheric Chemistry*, 75(1), 33-
796 70, doi:10.1007/s10874-017-9361-0.
- 797 Sun, K., Zhu, L., Cady-Pereira, K., Chan Miller, C., Chance, K., Clarisse, L., et al. (2018), A
798 physics-based approach to oversample multi-satellite, multispecies observations to a common
799 grid, *Atmospheric Measurement Techniques*, 11(12), 6679-6701, doi:10.5194/amt-11-6679-2018.
- 800 Sutton, M. A., Miners, B., Tang, Y. S., Milford, C., Wyers, G. P., Duyzer, J. H., & Fowler, D.
801 (2001), Comparison of low cost measurement techniques for long-term monitoring of
802 atmospheric ammonia, *Journal of Environmental Monitoring*, 3(5), 446-453,
803 doi:10.1039/b102303a.
- 804 Sutton, M. A., Reis, S., Riddick, S. N., Dragosits, U., Nemitz, E., Theobald, M. R., et al. (2013),
805 Towards a climate-dependent paradigm of ammonia emission and deposition, *Philosophical
806 Transactions of the Royal Society B-Biological Sciences*, 368(1621), 20130166,
807 doi:10.1098/rstb.2013.0166.
- 808 Tan, J., Fu, J. S., & Seinfeld, J. H. (2020), Ammonia emission abatement does not fully control
809 reduced forms of nitrogen deposition, *Proceedings of the National Academy of Sciences*,
810 117(18), 9771-9775, doi:10.1073/pnas.1920068117.
- 811 Tang, Y. S., Braban, C. F., Dragosits, U., Simmons, I., Leaver, D., van Dijk, N., et al. (2018),
812 Acid gases and aerosol measurements in the UK (1999-2015): regional distributions and trends,
813 *Atmospheric Chemistry and Physics*, 18(22), 16293-16324, doi:10.5194/acp-18-16293-2018.

- 814 ten Brink, H., Otjes, R., Jongejan, P., & Slanina, S. (2007), An instrument for semi-continuous
815 monitoring of the size-distribution of nitrate, ammonium, sulphate and chloride in aerosol,
816 *Atmospheric Environment*, *41*(13), 2768-2779, doi:10.1016/j.atmosenv.2006.11.041.
- 817 Tørseth, K., Aas, W., Breivik, K., Fjæraa, A. M., Fiebig, M., Hjellbrekke, A. G., et al. (2012),
818 Introduction to the European Monitoring and Evaluation Programme (EMEP) and observed
819 atmospheric composition change during 1972–2009, *Atmospheric Chemistry and Physics*,
820 *12*(12), 5447-5481, doi:10.5194/acp-12-5447-2012.
- 821 Twigg, M. M., Di Marco, C. F., Leeson, S., van Dijk, N., Jones, M. R., Leith, I. D., et al. (2015),
822 Water soluble aerosols and gases at a UK background site - Part 1: Controls of PM_{2.5} and PM₁₀
823 aerosol composition, *Atmospheric Chemistry and Physics*, *15*(14), 8131-8145, doi:10.5194/acp-
824 15-8131-2015.
- 825 UNECE (2019). *Annex I and II of the Gothenburg Protocol*. Retrieved from
826 [https://unece.org/DAM/env/documents/2017/AIR/Gothenburg_Protocol/Annex_II_and_III_upda](https://unece.org/DAM/env/documents/2017/AIR/Gothenburg_Protocol/Annex_II_and_III_updated_clean.pdf)
827 [ted_clean.pdf](https://unece.org/DAM/env/documents/2017/AIR/Gothenburg_Protocol/Annex_II_and_III_updated_clean.pdf)
- 828 Van Damme, M., Kruit, R. J. W., Schaap, M., Clarisse, L., Clerbaux, C., Coheur, P. F., et al.
829 (2014a), Evaluating 4 years of atmospheric ammonia (NH₃) over Europe using IASI satellite
830 observations and LOTOS-EUROS model results, *Journal of Geophysical Research:*
831 *Atmospheres*, *119*(15), 9549-9566, doi:10.1002/2014jd021911.
- 832 Van Damme, M., Clarisse, L., Heald, C. L., Hurtmans, D., Ngadi, Y., Clerbaux, C., et al.
833 (2014b), Global distributions, time series and error characterization of atmospheric ammonia
834 (NH₃) from IASI satellite observations, *Atmospheric Chemistry and Physics*, *14*(6), 2905-2922,
835 doi:10.5194/acp-14-2905-2014.
- 836 Van Damme, M., Clarisse, L., Dammers, E., Liu, X., Nowak, J. B., Clerbaux, C., et al. (2015a),
837 Towards validation of ammonia (NH₃) measurements from the IASI satellite, *Atmospheric*
838 *Measurement Techniques*, *8*(3), 1575-1591, doi:10.5194/amt-8-1575-2015.
- 839 Van Damme, M., Erismann, J. W., Clarisse, L., Dammers, E., Whitburn, S., Clerbaux, C., et al.
840 (2015b), Worldwide spatiotemporal atmospheric ammonia (NH₃
841) columns variability revealed by satellite, *Geophysical Research Letters*, *42*(20), 8660-8668,
842 doi:10.1002/2015gl065496.
- 843 Van Damme, M., Whitburn, S., Clarisse, L., Clerbaux, C., Hurtmans, D., & Coheur, P.-F.
844 (2017), Version 2 of the IASI NH₃ neural network retrieval algorithm: near-real-time and
845 reanalysed datasets, *Atmospheric Measurement Techniques*, *10*(12), 4905-4914,
846 doi:10.5194/amt-10-4905-2017.
- 847 Van Damme, M., Clarisse, L., Whitburn, S., Hadji-Lazaro, J., Hurtmans, D., Clerbaux, C., &
848 Coheur, P. F. (2018), Industrial and agricultural ammonia point sources exposed, *Nature*,
849 *564*(7734), 99–103, doi:10.1038/s41586-018-0747-1.
- 850 Van Damme, M., Clarisse, L., Franco, B., Sutton, M. A., Erismann, J. W., Wichink Kruit, R., et
851 al. (2021), Global, regional and national trends of atmospheric ammonia derived from a decadal
852 (2008-2018) satellite record, *Environmental Research Letters*, *16*(5), 055017, doi:10.1088/1748-
853 9326/abd5e0.
- 854 Vieno, M., Heal, M. R., Williams, M. L., Carnell, E. J., Nemitz, E., Stedman, J. R., & Reis, S.
855 (2016), The sensitivities of emissions reductions for the mitigation of UK PM_{2.5}, *Atmospheric*
856 *Chemistry and Physics*, *16*(1), 265-276, doi:10.5194/acp-16-265-2016.
- 857 Vitousek, P. M., Aber, J. D., Howarth, R. W., Likens, G. E., Matson, P. A., Schindler, D. W., et
858 al. (1997), Human alteration of the global nitrogen cycle: Sources and consequences, *Ecological*
859 *Applications*, *7*(3), 737-750, doi:10.1890/1051-0761(1997)007[0737:Haotgn]2.0.Co;2.

- 860 Vohra, K., Vodonos, A., Schwartz, J., Marais, E. A., Sulprizio, M. P., & Mickley, L. J. (2021a),
861 Global mortality from outdoor fine particle pollution generated by fossil fuel combustion:
862 Results from GEOS-Chem, *Environmental Research*, *195*, 110754,
863 doi:10.1016/j.envres.2021.110754.
- 864 Vohra, K., Marais, E. A., Suckra, S., Kramer, L., Bloss, W. J., Sahu, R., et al. (2021b), Long-
865 term trends in air quality in major cities in the UK and India: a view from space, *Atmospheric*
866 *Chemistry and Physics*, *21*(8), 6275-6296, doi:10.5194/acp-21-6275-2021.
- 867 Walker, H. L., Heal, M. R., Braban, C. F., Ritchie, S., Conolly, C., Sanocka, A., et al. (2019),
868 Changing supersites: assessing the impact of the southern UK EMEP supersite relocation on
869 measured atmospheric composition, *Environmental Research Communications*, *1*(0410011),
870 doi:10.1088/2515-7620/ab1a6f.
- 871 Walters, W. W., Chai, J., & Hastings, M. G. (2018), Theoretical phase resolved ammonia–
872 ammonium nitrogen equilibrium isotope exchange fractionations: Applications for tracking
873 atmospheric ammonia gas-to-particle conversion, *ACS Earth and Space Chemistry*, *3*(1), 79-89,
874 doi:10.1021/acsearthspacechem.8b00140.
- 875 Webb, J., & Misselbrook, T. H. (2004), A mass-flow model of ammonia emissions from UK
876 livestock production, *Atmospheric Environment*, *38*(14), 2163-2176,
877 doi:10.1016/j.atmosenv.2004.01.023.
- 878 Whitburn, S., Van Damme, M., Clarisse, L., Bauduin, S., Heald, C. L., Hadji-Lazaro, J., et al.
879 (2016a), A flexible and robust neural network IASI-NH₃ retrieval algorithm, *Journal of*
880 *Geophysical Research: Atmospheres*, *121*(11), 6581-6599, doi:10.1002/2016jd024828.
- 881 Whitburn, S., Van Damme, M., Clarisse, L., Turquety, S., Clerbaux, C., & Coheur, P. F. (2016b),
882 Doubling of annual ammonia emissions from the peat fires in Indonesia during the 2015 El Niño,
883 *Geophysical Research Letters*, *43*(20), 11007-11014, doi:10.1002/2016gl070620.
- 884 White, E., Shephard, M., Cady-Periera, K., Kharol, S., Dammers, E., Chow, E., et al. (2021),
885 Accounting for non-detects in satellite retrievals: Application using CrIS ammonia observations,
886 presented at EGU General Assembly, online, 19-30 April.
- 887 Wichink Kruit, R. J., Aben, J., de Vries, W., Sauter, F., van der Swaluw, E., van Zanten, M. C.,
888 & van Pul, W. A. J. (2017), Modelling trends in ammonia in the Netherlands over the period
889 1990–2014, *Atmospheric Environment*, *154*, 20-30, doi:10.1016/j.atmosenv.2017.01.031.
- 890 Zhu, L., Henze, D., Bash, J., Jeong, G. R., Cady-Pereira, K., Shephard, M., et al. (2015), Global
891 evaluation of ammonia bidirectional exchange and livestock diurnal variation schemes,
892 *Atmospheric Chemistry and Physics*, *15*(22), 12823-12843, doi:10.5194/acp-15-12823-2015.
- 893 Zhu, L., Jacob, D. J., Keutsch, F. N., Mickley, L. J., Scheffe, R., Strum, M., et al. (2017),
894 Formaldehyde (HCHO) as a hazardous air pollutant: Mapping surface air concentrations from
895 satellite and inferring cancer risks in the United States, *Environmental Science & Technology*,
896 *51*(10), 5650-5657, doi:10.1021/acs.est.7b01356.
- 897